

**THE DEVELOPMENT OF A DETAILED SEISMIC PERFORMANCE ASSESSMENT:  
A FRAMEWORK FOR CHINA'S HSR MSSS BRIDGE SYSTEM**

by

Xu Xie

B.A.Sc., The University of British Columbia, 2014

A THESIS SUBMITTED IN PARTIAL FULFILLMENT OF  
THE REQUIREMENTS FOR THE DEGREE OF

MASTER OF APPLIED SCIENCE

in

THE FACULTY OF GRADUATE AND POSTDOCTORAL STUDIES  
(Civil Engineering)

THE UNIVERSITY OF BRITISH COLUMBIA

(Vancouver)

April 2017

© Xu Xie, 2017

## **Abstract**

The Multi Span Simply Supported (MSSS) bridge system is the most commonly used structural system for High Speed Railway (HSR) networks in China. With China Railway rapidly expanding to the southwestern region of China, an area of high seismic activity, significant concerns have been raised to confirm whether the conventional HSR MSSS bridge, designed for low seismic zones, can be used in areas of high earthquake shaking intensities. In this thesis, the performance-based earthquake engineering (PBEE) methodology, originally developed for the seismic performance assessment of buildings, has been modified and applied to quantify the direct seismic loss of the China's HSR MSSS bridge system. This study is the first of its kind to systematically define and quantify the damage states, and associated repair actions, repair costs and travel delay losses for the China's HSR MSSS bridge system. The developed loss assessment model can be employed to assess the seismic performance of the HSR MSSS bridge system in diverse regions of China. In this study, a detailed parameter study using a framework developed in this thesis was utilized to study the influence of the shear capacity of fixed bearings on the seismic performance of a typical four-span HSR MSSS bridge system located in the Sichuan-Yunnan region in China. The results reveal that the financial loss of the HSR MSSS bridge system is highly dependent on the shear strength of the fixed bearing. Overall, the travel delay costs outweigh those for structural repair, where most of the financial loss was attributed to loss of functionality and repairs of the track-slab system and the bearings of the HSR MSSS bridge system. In addition, the developed fragility data and PBEE framework were used to optimize the design of the HSR MSSS bridge system using friction pendulum devices. The results show that

the most optimal seismic loss of the isolated HSR MSSS bridge system can be reduced by 90% when compared to the that in the absence of seismic isolation.

## **Preface**

The author of this thesis was responsible for the literature review, model development, data processing, and presentation of results. The manuscripts were drafted by the author of the thesis and revised based on comments by Professor T.Y. Yang at the University of British Columbia and Professor Guo Wei at Central South University, China.

# Table of Contents

<b>Abstract.....</b>	<b>ii</b>
<b>Preface.....</b>	<b>iv</b>
<b>Table of Contents .....</b>	<b>v</b>
<b>List of Tables .....</b>	<b>viii</b>
<b>List of Figures.....</b>	<b>ix</b>
<b>List of Symbols .....</b>	<b>xi</b>
<b>List of Abbreviations .....</b>	<b>xiii</b>
<b>Acknowledgements .....</b>	<b>xv</b>
<b>Dedication .....</b>	<b>xvi</b>
<b>Chapter 1: Introduction .....</b>	<b>1</b>
1.1 Overview.....	1
1.2 Research Objectives.....	2
1.3 Thesis Outline .....	3
<b>Chapter 2: Literature Review .....</b>	<b>5</b>
2.1 The Characteristics of HSR MSSS Bridges in China .....	5
2.1.1 Bridge Girders.....	5
2.1.2 The CRTS II Track-Slab System .....	7
2.1.3 Bridge Piers.....	8
2.1.4 Bridge Bearings .....	9
2.2 Development of the Performance Evaluation Framework for MSSS Bridges .....	11

2.3	Summary .....	14
<b>Chapter 3: Seismic Performance of the HSR MSSS Bridge System.....</b>		<b>15</b>
3.1	A Description of the Analytical Model for the HSR MSSS Bridge System .....	15
3.1.1	MSSS Bridge Pier Modeling .....	16
3.1.2	MSSS Bridge Bearings Modeling and the Element Removal Technique .....	17
3.1.3	The MSSS Bridge Girder and Joint Modeling.....	20
3.2	Seismicity and Ground Motion Selection .....	21
3.3	Seismic Responses of the Four-Span HSR MSSS Bridge Model.....	24
3.4	Summary .....	28
<b>Chapter 4: The Performance-based Methodology for Evaluating the Multi-Span Simply Supported Bridge Response .....</b>		<b>29</b>
4.1	Performance Groups .....	29
4.2	Damage and Loss Analysis.....	30
4.2.1	HSR MSSS Bridge Pier Performance Groups .....	32
4.2.2	Bearing Performance Groups.....	33
4.2.3	Track-slab Performance Group.....	35
4.2.4	Roadbed Performance Group.....	36
4.2.5	Damage Fragility Curves .....	37
4.3	Seismic Performance Evaluation .....	38
4.3.1	The Cumulative Distribution Function of TSR and TTD costs .....	39
4.3.2	The De-aggregation of the TSR and TTD Costs .....	40
4.3.3	Time-based Assessments .....	43
4.4	Summary .....	44

<b>Chapter 5: Seismic Performance Evaluations and Optimizations of the HSR MSSS Bridge Using the Friction Pendulum System</b> .....	<b>46</b>
5.1 Literature Review of the FPS and its Optimal Design Methodologies.....	46
5.2 A Model Description of the FPS.....	49
5.3 A Model Description of the Isolated four-span HSR MSSS bridge .....	53
5.4 Allowable Ranges of Design Parameters of the FPS.....	55
5.4.1 The Boundary Conditions Imposed by the FPS.....	55
5.4.2 The Boundary Condition Imposed by Girder Joints .....	58
5.4.3 The Boundary Condition Imposed by the Piers .....	60
5.5 The Optimized Ranges of the Design Parameters of FPS .....	61
5.6 Summary .....	64
<b>Chapter 6: Summary and Conclusion</b> .....	<b>65</b>
6.1 Summary and Conclusion .....	65
6.2 Future Research .....	66
<b>Bibliography</b> .....	<b>68</b>
<b>Appendices</b> .....	<b>74</b>
Appendix A : Additional Design Parameters for the FPS .....	74
A.1 The Radius Curvature of the FPS .....	74
A.2 Uplift of the FPS .....	74
A.3 The Maximum Allowable Longitudinal Displacement of FPS .....	75

## List of Tables

Table 1 Fundamental vibration periods of the typical four-span HSR MSSS bridge.....	21
Table 2 Summary of performance groups .....	30
Table 3 Repair methods and corresponding bridge closure times .....	31
Table 4 Damage states of HSSS HSR pier (obtained from Jiang et al. 2013).....	32
Table 5 Repair quantities and unit costs for the pier PG .....	33
Table 6 Damage states and fragility curves for fixed and sliding bearing.....	34
Table 7 Repair quantities and unit costs for bearing PGs.....	34
Table 8 Median EDP and dispersion ( $\beta$ ) values for reaching each DS of the track-slab PGs .....	35
Table 9 Repair quantities and unit costs of the track-slab PGs.....	35
Table 10 Median EDP value for reach each DS of the roadbed PGs .....	36
Table 11 Repair quantities and unit costs of roadbed PGs .....	37
Table 12 Median CDF cost of each case .....	40
Table 13 A Parametric study of the FPS with different sets of values for $TR$ and $\mu$ .....	53
Table 14 Loss analysis of FPS .....	54
Table 15 Damage analysis of track PG with FPS .....	54
Table 16 The calculated $D_{Lm}$ [mm] for each of the $TR$ .....	56
Table 17 A comparison of seismic performances of the prototype HSR MSSS bridge with and without FPS.....	63
Table 18 The radius of curvature of the FPS w.r.t to each TR ratio.....	74
Table 19 Uplift w.r.t to each TR ratio.....	75
Table 20 The calculated $D_{Lm}$ [mm] values for each of the $TR$ .....	75



## List of Figures

Figure 1 Typical HSR MSSS bridges in China (Authorized by Huitu.com).....	1
Figure 2 Cross-section of a box girder beam with double HSR lines [mm].....	6
Figure 3 Cross-section of CRTS II non-ballasted track-slab system.....	7
Figure 4 Schematic diagram of rectangular bridge piers with rounded-ends .....	8
Figure 5 Longitudinal cross-section of the steel spherical bearings of the HSR MSSS bridge....	10
Figure 6 Cross-sectional views of the bridge girder and its supporting bearings.....	11
Figure 7 Four analysis phases of the PBEE framework (permission granted by Yang et al., 2009) .....	12
Figure 8 Elevation view of a two-dimensional numerical model of a four-span HSR MSSS bridge .....	16
Figure 9 Cyclical pushover test of a 16-meter height HSR bridge pier at 1-to-8 ratio (Jiang et al, 2013).....	17
Figure 10 Material properties for simulating bridge bearings .....	18
Figure 11 The procedures of direct element removal for each fixed bearing.....	19
Figure 12 Material properties for the element of girder joints in OpenSees. ....	20
Figure 13 China’s seismic hazard maps of the PGA zonation at 10% in 50 years (Permission from Wu et al. 2017).....	22
Figure 14 Design spectrum and ground motions for each hazard level.....	23
Figure 15 Median peak drift developed at piers .....	25
Figure 16 Median peak longitudinal relative displacement developed at bearings .....	26
Figure 17 Median peak tensile and compressive displacement developed at girder joints .....	27

Figure 18 The location of each type of EDPs of the 21 PGs of the typical four-span HSR MSSS bridge .....	30
Figure 19 Damage fragility curves for each PG of the prototype bridge model.....	38
Figure 20 Cumulative distribution function of total monetary loss .....	40
Figure 21 De-aggregation of TSR cost for each performance group.....	42
Figure 22 De-aggregation of TTD cost for each performance group .....	43
Figure 23 Loss curves and corresponding MAL values for each bridge model. ....	44
Figure 24 Free body diagram of a single concave FPS .....	49
Figure 25 De-aggregation of hysteresis behaviors of FPS.....	51
Figure 26 Hysteresis model for the single concave FPS.....	52
Figure 27 Schematic diagram of an isolated four-span HSR MSSS bridge .....	53
Figure 28 Modified fragility curves for related PG of the isolated four-span HSR MSSS bridge	55
Figure 29 The plots of median longitudinal peak displacement of R-FPS vs. $TR$ and $\mu$ .....	57
Figure 30 The boundary condition of $TR$ and $\mu$ imposed by the uplift of the FPS .....	58
Figure 31 3-D plots of the median peak displacements of the girder joints (compressional) vs. $TR$ and $\mu$ .....	59
Figure 32 The boundary conditions of $TR$ and $\mu$ imposed by the EDP limit of the girder joints.	60
Figure 33 The 3-D plots of the longitudinal median peak pier-top displacement vs. $TR$ and $\mu$ ..	61
Figure 34 TML vs. $TR$ and $\mu$ of FPSs under MCE, DBE and SLE levels of ground motions. ....	63

## List of Symbols

- $a/d$  : aspect ratio
- $f_c$  : characteristics compressive strength
- $Q$  : characteristics force of the hysteresis of FPS
- $\mu$  : coefficient of friction
- $F_{max}$  : coulomb friction force of bridge bearings
- $\beta$  : dispersion ratio
- $F_f$  : frictional force of FPS
- $T_1$  : fundamental vibration period of structure
- $D_L$  : longitudinal displacement of FPS
- $\rho_l$  : longitudinal reinforcement ratio
- $M_w$  : magnitude of earthquake
- $x_y$  : maximum allowable static deformation of bearings
- $N$  : normal force
- $R$  : radius of curvature of FPS
- $\theta$  : rotational angle of FPS
- $F_{shear}$  : shear strength of the fixed bridge bearings
- $v_{30}$  : shear wave velocity of soil at 30 meter below grade
- $\rho_s$  : stirrup ratio
- $A_g$  : stirrup ratio

$D_{up}$  : uplift of FPS

$X_1$  : width of girder joint

## List of Abbreviations

CA	: cement asphalt
CDF	: cumulative distribution function
DBE	: continuous welded
DS	: damage state
EDP	: engineering demand parameter
FORM	: first-order reliability theorem
FPS	: friction pendulum system
HSR	: high-speed railway
IDA	: incremental dynamic analysis
MAL	: mean annual total value of loss
MCE	: maximum considered earthquake
MSSS	: multi-span and simply supported
PBEE	: performance-based earthquake engineering
PG	: performance group
PSDA	: probabilistic seismic demand analysis
PSDM	: probabilistic seismic demand model
RC	: reinforced concrete
SLE	: service level earthquake
TML	: total monetary loss

TSR : total structural repair

TTD : total travel delay

TR : isolation ratio of FPS

CR : China Railway

CWR : continuous welded rail

IM : intensity measure

PEER : Pacific Earthquake Engineering Research center

ADR : average daily revenue

AUC : average unit cost

ARE : annual rate of exceedance

## **Acknowledgements**

I would like to express my gratitude to Professor T.Y. Yang for his unreserved coaching, insightful inspiration and immense encouragement. Likewise, my immeasurable appreciation is expressed to Professor Wei Guo, Professor Biao Wei and Professor Lizhong Jiang from Central South University in China for their invaluable advice. It has been my pleasure to successfully complete this work with the additional encouragement and support of my friends and associates, Dr. Dorian Tung, Yuanjie Li, Jason Lin, Yuxin Pan, Lisa Tobber and Ming Yang. I accord further appreciation to my classmates, Tianci Wang, Xiang Li and Yu Feng. First and foremost, I would like to extend my ineffable acknowledgement towards my parents for their unconditional support.

## Dedication

*To my parents*



# Chapter 1: Introduction

## 1.1 Overview

The High Speed Railway (HSR) has seen an unprecedented construction boom worldwide, and particularly in China over the last decade. As of August 2016, a total 20,000 km of Chinese HRS has been in operation with a daily ridership of over 4.0 million (Smith 2017). Another 15,000 km of HSR lines is scheduled to be constructed by the end of 2025 (The Economist 2017). More than 50% of the HSR lines have been constructed over bridges, with 90% of these bridges are constructed using the Multi Span Simply Supported (MSSS) box girder bridge systems (Yan et al. 2015). Figure 1 shows a typical construction layout of the MSSS in China.



**Figure 1 Typical HSR MSSS bridges in China (Authorized by Huitu.com)**

With the population growth taking place in the southwest region of China, the China Rail (CR) company has determined to expand its HSR network into that region. The southwest China is a region of high seismic activity, where the active Tibetan plateau meets with South China plain. In 2008, the Wenchuan earthquake struck this region, killing over 70,000 people and resulting in a 1.5 trillion RMB direct economic loss (Yong and Booth 2011). This was one of the most devastating earthquakes in modern Chinese history. Significant concerns have been raised to

determine whether the HSR MSSS bridge, which was originally designed for low seismic zones, could also be used in areas of significant earthquake agitation. To address this concern, the advanced Performance Based Earthquake Engineering (PBEE) evaluation framework, originally developed by Yang et al. (2009) for the performance assessment of buildings under seismic load, has been modified to ascertain the seismic performance of HSR MSSS bridges in the Sichuan-Yunnan region. To properly account for the seismic vulnerability of the HSR MSSS bridges, the interactions between structural components, such as piers, girders and bearings, and non-structural components like the track-slab system were taken into account. The total monetary loss of a typical four-span HSR MSSS bridge with and without consideration for the travel delay loss was calculated. The results and the framework as presented in this study can be utilized to assess the seismic vulnerability of HSR MSSS bridge systems, which will enable decision makers to select the most suitable retrofitting scheme to improve the seismic performance of the HSR bridge system.

## **1.2 Research Objectives**

The research presented in this thesis aims to achieve the following three objectives:

1) Develop detailed analytical models to simulate the seismic response of the China HSR MSSS bridge system. In this model, the detailed interactions between such key bridge components as bridge bearings, box girders and the non-ballasted track system are explicitly accounted for.

2) Detailed failure mechanisms of the critical components of the China's HSR MSSS bridge system are defined. The damage state, repair actions, repair costs and repair time are employed to conduct a systematic performance-based evaluation according to the PBEE framework presented in this thesis. The damage states, fragility data, repair actions, repair costs

and travel delay loss are clearly defined based on a thorough investigation of the related experimental data, design codes, engineering drawings and original construction procedures.

3) Apply the PBEE framework to optimize the design of the friction pendulum system (FPS) for the China HSR MSSS bridge system. This innovative optimal design methodology will minimize losses of the HSR MSSS bridge system by considering these losses under multiple hazard levels.

### **1.3 Thesis Outline**

The seismic responses, performance-based evaluation and optimal design of isolation devices for the China HSR MSSS bridge system are discussed in the following chapters:

Chapter 2 provides a detailed investigation of the structural characteristics of key components of the China HSR MSSS bridge system and discusses its potential failure mechanisms. In addition, this chapter reviews the basic mechanism of the PBEE framework and its past implementation on bridge structures.

Chapter 3 presents the finite-element model of a typical four-span HSR MSSS bridge with fixed bearings at five level of shear strength. It also presents details of modeling techniques for each key component of the China HSR MSSS bridge system. The finite element model, which takes into account the pounding effects between its adjacent girders, employs a modified girder joint element. Additionally, the fracture of fixed bearings at different levels of shear strength was simulated using a direct element removal technique in OpenSees.

Chapter 4 presents a systematical performance-based evaluation of the typical four-span HSR MSSS bridge. The bridge system was divided into several key performance groups (PGs). For each PG, the damage states and corresponding fragility data were defined based on past

experimental data and available design codes. Loss analysis for each PG was conducted based on the cost of the past bridge retrofit and current HSR construction costs. The results of this performance-based evaluation are presented in terms of Total Structural Repair (TSR) and Total Travel Delay (TTD) costs and Total Monetary Loss (TML). The results of the loss analysis are presented in terms of the Cumulative Distribution Function (CDF) of total loss, and a de-aggregation of the total cost for each PG, loss curve and Mean Annual Total Value of Loss (MAL).

Chapter 5 presents an optimization design of the friction pendulum system (FPS) for the HSR MSSS bridge system, which was conducted using the PBEE framework. The design parameters of the FPS were selected to achieve the minimum TML. The performance of FPS equipped isolated bridges with or without shear rods was also compared. In addition, the relationships between the key engineering demand parameters (EDPs) and design parameters of the FPS have been quantified using the PBEE framework. The strict displacement-based design criteria and conflict responses between the FPS and the piers were evaluated based on these relationships.

Chapter 6 presents a summary of research findings, a conclusion and recommendations for future studies on the evaluation of HSR MSSS bridge systems.

## **Chapter 2: Literature Review**

The purpose of this chapter is to identify the structural characteristics and potential failure mechanisms of the key structural and non-structural components of the HSR MSSS bridge system. In addition, interactions between each key bridge component and the boundary conditions of the bridge are described. As well, this chapter introduces the basic mechanism of the PBEE framework and provides a literature review of past studies using performance-based evaluation methods to assess the seismic safety of bridge structures.

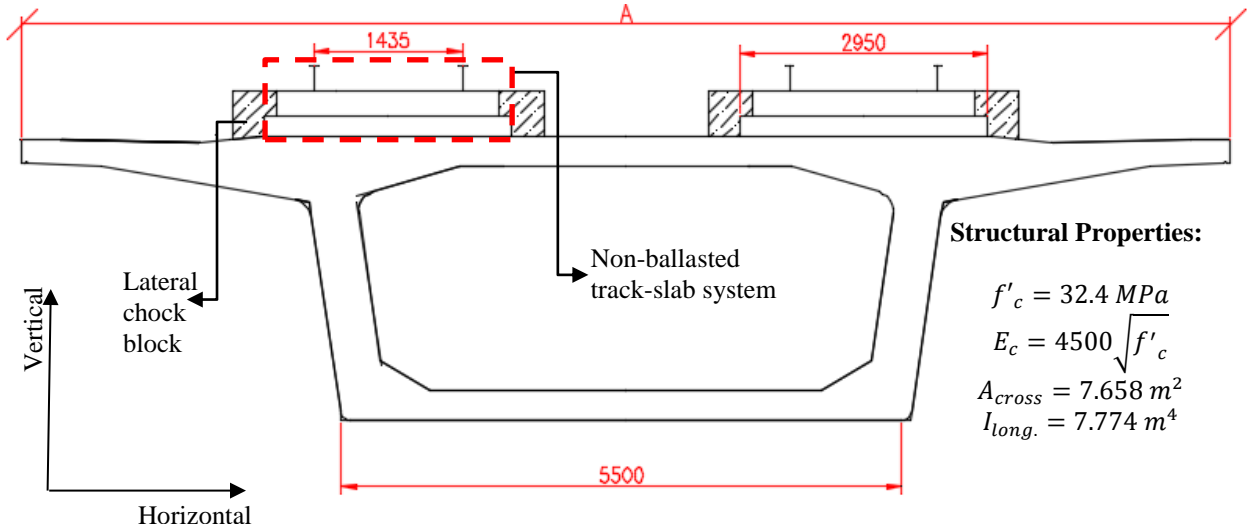
### **2.1 The Characteristics of HSR MSSS Bridges in China**

The MSSS bridge system has frequently been employed for use as elevated viaducts for China's HSR lines traversing flat areas in order to preserve arable lands in the countryside and minimize impacts on suburban areas. Hence, the bridge-to-track ratio in China's HSR is much higher than the equivalent ratios in European countries. For example, 956 km of the total 1318 km of the Beijing-Shanghai HSR line are constituted by HSR MSSS bridges (Sun 2008). The lengths of these MSSS bridges range from 32 meters to 165 km. With the increasing number of spans, the constraint effect imposed by abutment and roadbed on the excessive movement of the middle span of the bridges is diminished. Hence, a four-span HSR MSSS prototype bridge with piers of 16 m height was selected for this study.

#### **2.1.1 Bridge Girders**

Figure 2 shows the cross-section of a typical box girder used in China's HSR MSSS bridge system. This box girder has a clear span of 31.5 meters and a self-weight of 900 metric tonnes. It

has been designed to achieve a high degree of stiffness in order to strictly control for deflection and vibration. Field experimental tests, which confirmed the immense stiffness of the box girder, disclosed a fundamental frequency of 6.7 Hz and maximum vertical deflection of  $L/9090$  under operation load (Hu et al. 2013). The girder deck has a width of 13.4 meters, which is designed to support two track-slab systems at an operation speed of 350 km/hour. Twelve lateral concrete chock blocks are placed at each side of the track-slab system per girder to minimize the vertical and horizontal movements of that system when the HSR train travels across the bridge. The total weight of the girder (including all non-structural members at the tops of the girders) ranges from 1250 to 1500 metric tonnes.

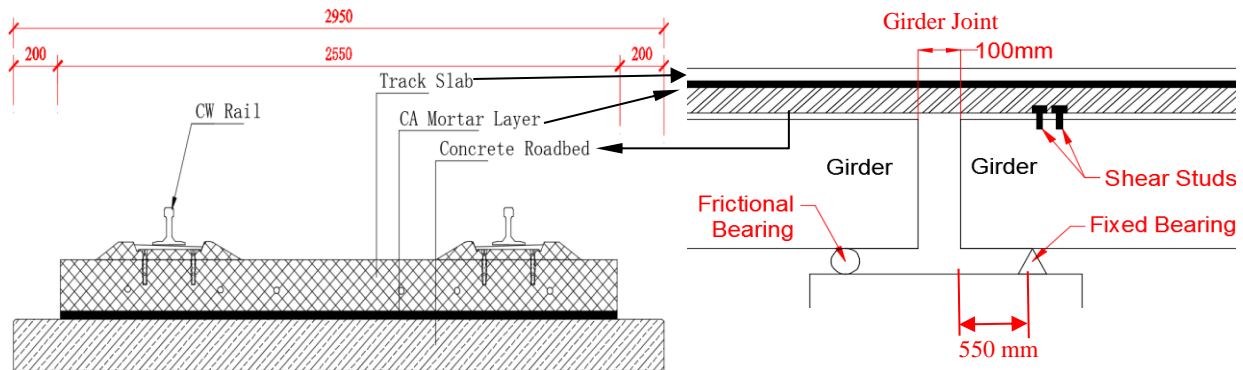


**Figure 2 Cross-section of a box girder beam with double HSR lines [mm]**

To minimize defective workmanship and maximize productivity in construction, all girders are pre-fabricated in factories on construction sites. Following a proper curing and quality inspection of the girders, the girder will be moved directly from the factory to the railway line and installed by special girder-erecting machinery.

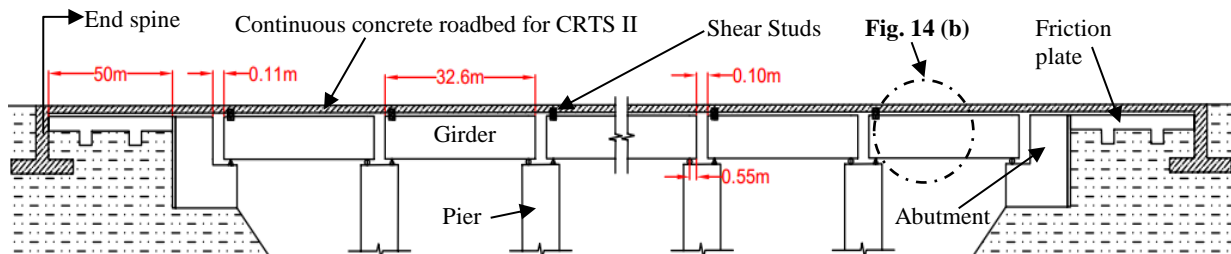
### 2.1.2 The CRTS II Track-Slab System

Figure 3(a) demonstrates that CRTS II track-slab system is commonly used as the non-ballasted track-slab system. A CRTS II track-slab system consists of four key components: 1) Continuous Welded Rail (CWR), 2) Track slabs, 3) Cement Asphalt (CA) mortar layers, and 4) Concrete roadbeds. The roadbed is connected to the girder through shear studs as shown in Figure 3(b). It should be noted that there is a 100-mm physical gap between two consecutive girders (as shown in Figure 3b). This gap is reserved for thermal expansion and any relative movement between the girders. If the relative movement of the girder is large, then the CRTS II track-slab system could be damaged. The CWR, track slab and CA mortar layer are continuous for the entire span of the high-speed rail line, while the concrete roadbed is only continuous up to the end span of the bridge. Figure 3(c) shows the assembly of a typical HSR MSSS bridge system.



(a) Cross section of CRTS II track-slab system

(b) Track-slab system across one girder joint



(c) The side view of a typical HSR MSSS bridge

**Figure 3 Cross-section of CRTS II non-ballasted track-slab system**

### 2.1.3 Bridge Piers

Figure 4 shows a typical pier used for HSR MSSS bridges. The height of the pier can range from 4 to 24 meters. The HSR MSSS pier is stockier than conventional railway MSSS piers, it is usually over-designed to achieve the stiffness required to ensure that the HSR can operate at high speeds with minimal deformation and vibration. The piers also need to possess sufficient strength to overcome the braking force from the HSR, which is eight times higher than that on highway bridges (Aparicio 2008). In addition, the design of the HSR pier needs to ensure that the maximum deformation under the braking force in the longitudinal direction of the bridge is limited to 4 mm (CRC 2012). Hence, the sections for the HSR MSSS bridge are typically designed using solid concrete pier.

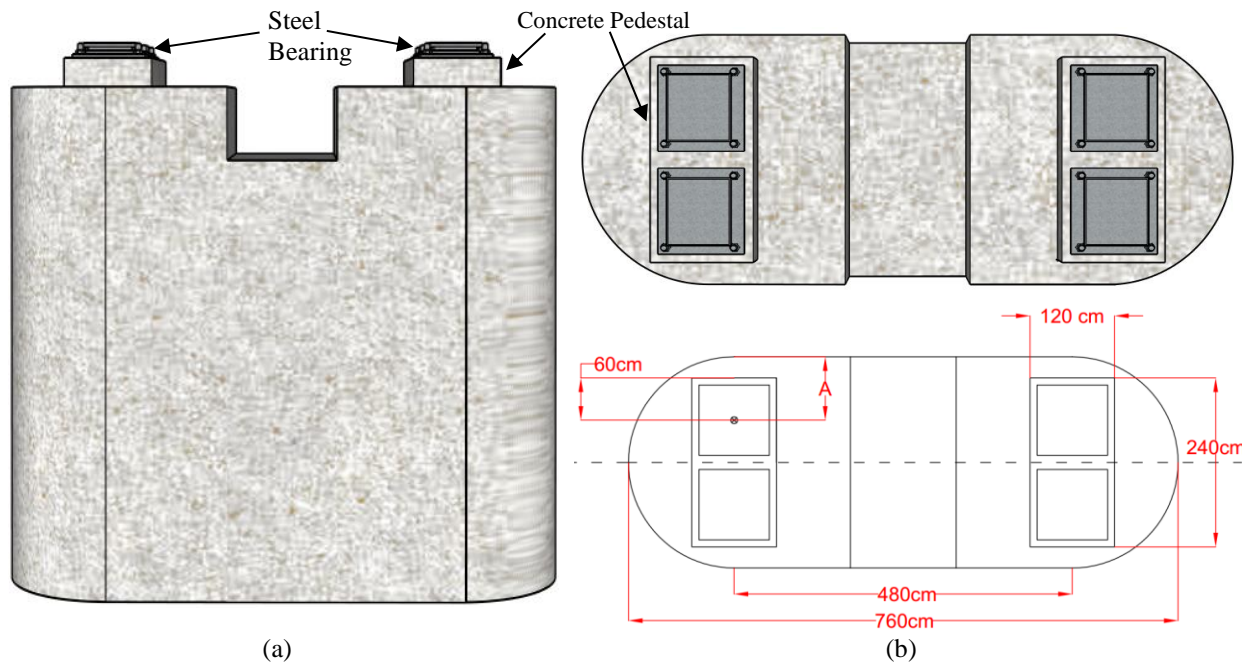
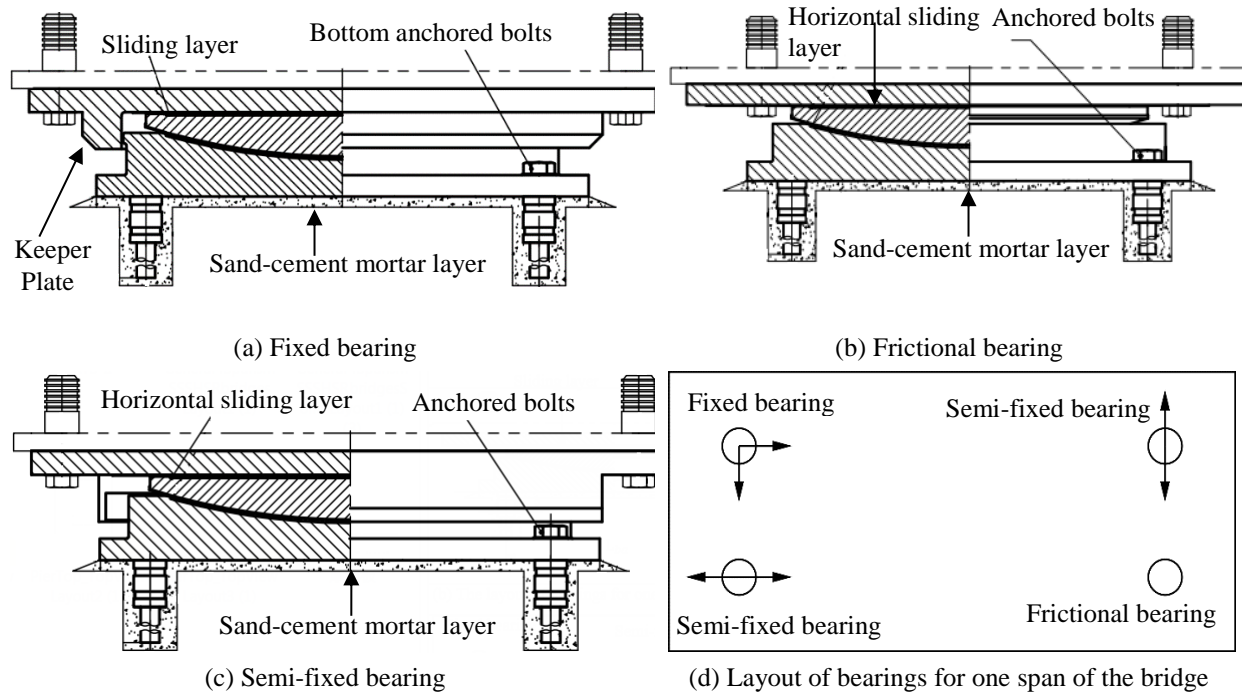


Figure 4 Schematic diagram of rectangular bridge piers with rounded-ends



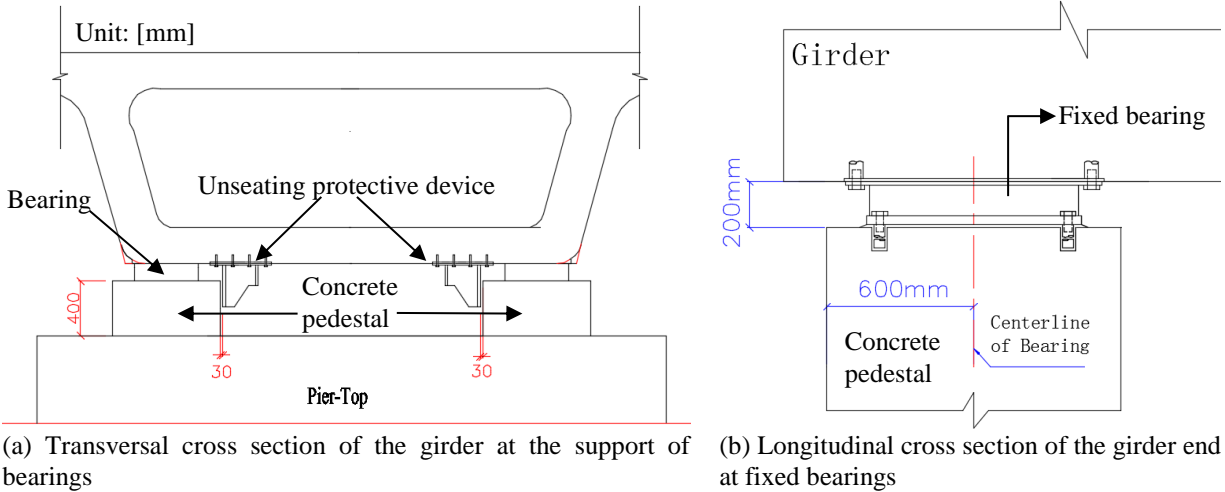
#### 2.1.4 Bridge Bearings

Figure 5 illustrates the typical bearings used for an HSR MSSS bridge. Figure 5(a) shows the typical fixed steel spherical bearing employed in the HSR MSSS bridge. It is designed based on the strong bearing and weak anchors principle (China CR 2006). In other words, the bottom anchors are designed to be weaker than the top ones. Hence, the failure mode of the bearing is seen in the fracture at lowermost anchors. Based on the standardized design of the steel spherical bearing, the design bearing strength (fracture strength of the lower anchor) in the case of the 32-m box girder is between 750 to 2800 kN. Figure 5(b) illustrates the frictional bearing. In this type of bearing, the bearing is designed to slide when the shear force exceeds 122.8 kN (0.02 W) in either direction. Figure 5(c) displays the semi-fixed bearing. This type of bearing acts as the fixed bearing, in the direction in which the motion is restrained. In the direction where the motion is unrestricted, the bearing acts as a friction bearing. The layout of these types of bearings for supporting single-span of the HSR MSSS bridge is shown in Figure 5(d), with the arrows demonstrating the direction of the restraint provided by each bearing. In this thesis, the longitudinally fixed bearing is termed the fixed bearing, while the longitudinal unrestrained bearing on the alternate side of the girder is labelled the frictional bearing.



**Figure 5 Longitudinal cross-section of the steel spherical bearings of the HSR MSSS bridge**

Moreover, lateral excessive movement in transverse direction of the superstructure is also restrained by unseating the protective devices, as shown in Figure 6(a). However, the longitudinal excessive movement of the superstructure is only restrained by the fixed bearings, as shown in Figure 6(b). The centerline of the fixed bearing is placed 60 cm from the edge of its supporting concrete pedestal, as illustrated in Figure 6. Hence, when the relative movement between the bearing and concrete pedestal exceeds 60 cm, the desk is expected to unseat. This type of unseating failure will not create global collapse, but it will easily damage the track-slab system and create the excessive alignment issue for CW rail. It should be noted this failure mode is currently not considered in the conventional seismic design code.



**Figure 6 Cross-sectional views of the bridge girder and its supporting bearings**

## 2.2 Development of the Performance Evaluation Framework for MSSS Bridges

Multiple studies have been developed in the past to assess the seismic safety of general highway bridge structures. Mackie (2003) investigated the optimal pairs of Intensity Measure (IM) and Engineering Demand Parameter (EDP) for fragility functions of highway bridges. Their results show the performance of the highway bridge is correlated to the column drift ratio. In other words, a reduction of the column drift ratio will be the most effective means to improve the performance of the highway MSSS bridge. Choi et al. (2004) developed more detailed system fragility curves to assess the performance of general multi-span highway bridges. In their study, they combined the analytical component fragility curves through the first-order reliability theorem (FORM) by assuming the MSSS bridge is a series system. Kim et al. (2006) point out that the global seismic behaviour of highway MSSS bridges is highly dependent on the performance of the bearings. Hence, the system fragility function of highway MSSS bridges should account for both the pier and bearing damages. Zhang and Huo (2009) propose that a relative important ratio of 0.75 and 0.25 should be assigned to the pier and bearing, respectively.

The above mentioned studies focus on the performance evaluation of highway MSSS bridges in terms of probability of failure, but it is difficult for non-engineers to make informed risk management decisions. To address this deficiency, the performance-based earthquake engineering (PBEE) evaluation framework originally developed by the Pacific Earthquake Engineering Research (PEER) Center and further improved by Yang et al. (2009) and FEMA P-58 (FEMA 2012) has been used in this study to assess the seismic vulnerability of highway bridges. The PBEE framework divides the seismic performance assessment into four analysis phases, as shown in Figure 7. These include: the seismic hazard analysis, the response analysis, the damage analysis and the loss analysis. The seismic hazard analysis focuses on a quantification of the seismic hazards at the site while the response analysis focuses on the structural and non-structural component responses under different levels of earthquake shaking intensities. The damage analysis focuses on the quantification of the structural and non-structural component damages based on structural and non-structural component responses. Lastly, the loss analysis translates the structural and non-structural component damages into financial losses or other decision variables which can be used for risk management. The uncertainties within each of the analysis phase are integrated using total probability as shown in Equation 1.

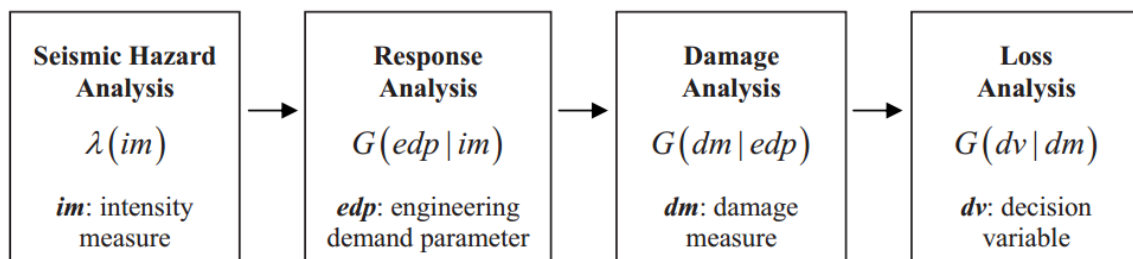


Figure 7 Four analysis phases of the PBEE framework (permission granted by Yang et al., 2009)

$$v(DV > dv) = \int_{im} \int_{dm} \int_{edp} G(dv|dm)dG(dm|edp)dG(edp|im)|d\lambda(im) \quad (1)$$

Ketchum (2004) present the detailed repair actions and repair costs of typical high way bridge components at different damage states. Mackie et al. (2008) used the data presented by Ketchum (2004) and the PBEE framework to calculate the total structural repair costs of a five-span prototype highway MSSS bridge in California. In this study, the travel delay cost which is the most significant decision variable was not included in the assessment. Later, Terzic and Stojadinovic (2010) thoroughly studied the post-earthquake traffic capacity of highway bridges, where the down time of the highway bridge was considered. In this paper, a detailed PBEE assessment of HSR MSSS bridges was assessed using the framework presented in Figure 1. It should be noted that the design and functionality of the HSR MSSS bridge is very different from that of the conventional highway MSSS bridge. The HSR MSSS bridge system is highly engineered for its construction efficiency, where the structures are designed to provide a high degree of stiffness to ensure the HSR can operate smoothly at high operating speed. More importantly, the HSR MSSS bridge consists of a continuously welded rail (CWR) and a non-ballasted track-slab system (CRTS-II), which are unique to the HSR MSSS bridge. In this thesis, the key structural and non-structural components and their associated damage states, repair actions and repair costs for the HSR MSSS bridge systems are clearly presented. In addition, the repair time and associated travel costs are included in the PBEE assessment. The presented fragility curves and associated repair actions and costs can be used to assess the seismic performance of other HSR MSSS bridges in other regions.

### 2.3 Summary

The structural characteristics of the HSR MSSS bridge have been presented in this chapter. It has been determined that the bottom anchor bolts of fixed bearing are vulnerable to seismic loads. Hence, bearing unseating failure is the major potential failure mechanism, as it directly impacts the alignment of the track-slab system and the functionality of HSR lines. In addition, longitudinally excessive relative movement between girders is another potential failure mechanism which will damage the continuous roadbed and track-slab system.

Moreover, past seismic performance assessments of bridge structures have been reviewed. This review shows that the focus of the probabilistic evaluation community has gradually shifted from the failure probability to direct financial loss due to different hazard levels of ground motion. However, most past studies do not take into account travel delay loss, which constitutes a large portion of seismic financial loss. In addition, past studies usually relate the functionality of bridges to the loading capacity of the piers, which cannot be applied to HSR bridges.

## **Chapter 3: Seismic Performance of the HSR MSSS Bridge System**

The purpose of this chapter is to develop a robust analytical model to simulate the longitudinal seismic responses of a typical four-span HSR MSSS bridge under different levels of earthquake shaking intensity. Detailed modeling approach of key structural components were calibrated from experimental data. The seismic performance of a prototype four span HSR MSSS bridge located in the Yunnan-Sichuan region was assessed. Eighteen ground motions were selected and scaled to match the seismic spectrum for the location of the prototype bridge. In addition, a direct element removal technique has been implemented to model the fixed bearing at different levels of shear strength.

### **3.1 A Description of the Analytical Model for the HSR MSSS Bridge System**

A two-dimensional four-span HSR MSSS bridge system was numerically modeled using OpenSees (PEER 2017), as presented in Figure 8. The nonlinear behaviors of this bridge system were mainly simulated in the substructure and in the expansion joints between its adjacent girders. Cyclic pushover testing data was introduced to calibrate the bridge piers, and an advanced element removal technique was applied to model the fractured fixed bearings. Moreover, a modified gap element was employed to simulate the pounding effect at each expansion joint. The response of this MSSS bridge model will be analyzed to gain insight into its system's seismic behavior, which will facilitate further performance evaluations and the formulation of an optimal design methodology.

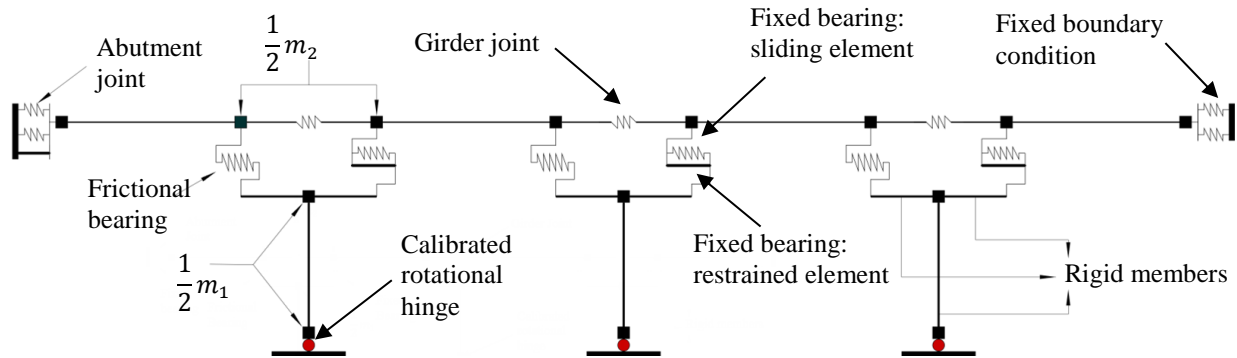


Figure 8 Elevation view of a two-dimensional numerical model of a four-span HSR MSSS bridge

### 3.1.1 MSSS Bridge Pier Modeling

Nonlinear behaviors in RC columns and piers have been experimentally investigated for several decades, providing a database for researchers, who have developed constitutive models of confined concrete material to simulate nonlinearity. Most of the widely accepted constitutive models were derived from the experimental data of RC concrete specimens, at an aspect ratio ( $a/d$ ),  $1 \leq a/d \leq 4$ , and a longitudinal reinforcement ratio ( $\rho_l$ ),  $1\% \leq \rho_l$  (e.g., (Mander et al. 1988), (Hoshikuma et al. 1997) and (Sezen and Moehle 2004)). However, the existing constitutive models cannot sufficiently represent the nonlinear behaviors of the solid RC piers of HSR bridges, because the piers usually have a higher aspect ratio ( $a/d$ ),  $5 \leq a/d \leq 8$ , and a lower longitudinal reinforcement ratio ( $\rho_l$ ),  $\rho_l \leq 1\%$ . Shao and Jiang (2014) reveal that it is difficult to use the Kent-Scott-Park model (Scott et al. 1982), Mander model (P. Mander et al. 1989) and Modified Chang-Mander Model (Waugh 2009) to capture the nonlinear behaviors of the HSR piers under the cyclical pushover test, especially due to pinching effects and degradations of strength.



Hence, the nonlinear behavior of the piers was directly calibrated using the experimental data of cyclical pushover tests on solid piers with a rounded rectangular cross-section in the China HSR bridge (Jiang et al. 2013). The pier of the HSR MSSS bridge was modeled using a rigid beam with a zero-length rotational element at its base. Hysteretic material with pinching effects and degradations was chosen for the rotational element in OpenSees. The testing results for the 16-m specimen, at a 1-to-8 ratio, were selected for the calibration. The simulated force-deformation response of the pier obtained through the experimental and numerical simulation is shown in Figure 9.

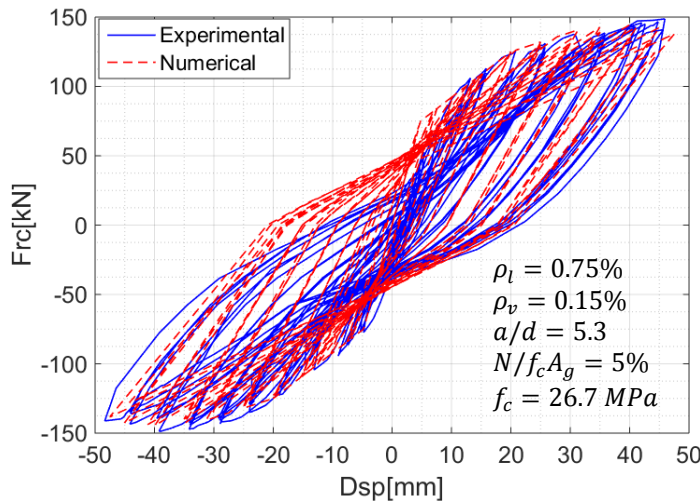
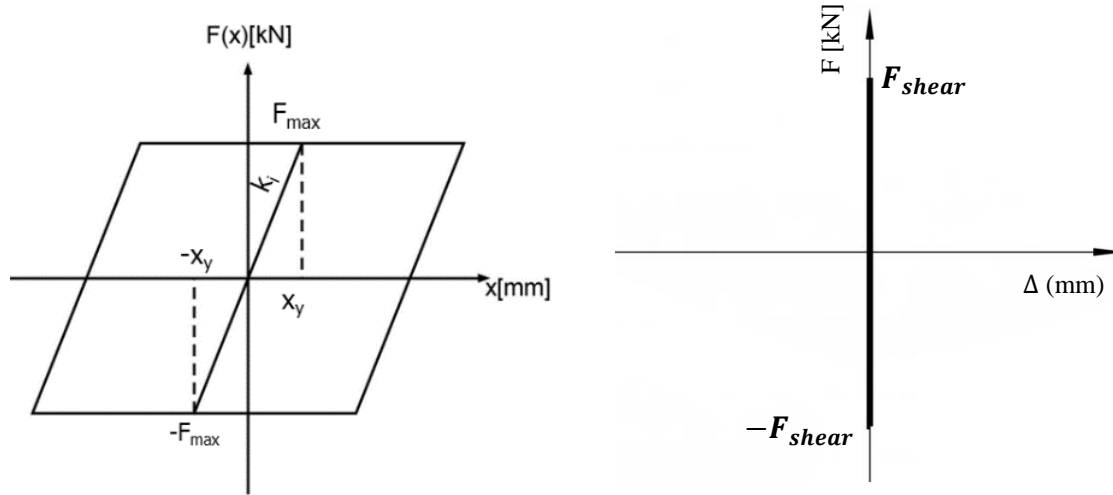


Figure 9 Cyclical pushover test of a 16-meter height HSR bridge pier at 1-to-8 ratio (Jiang et al, 2013)

### 3.1.2 MSSS Bridge Bearings Modeling and the Element Removal Technique

All varieties of bridge bearings were simulated using zero-length spring elements with an elastic-perfectly-plastic material property, as shown in Figure 10(a). The friction coefficient ( $\mu$ ) of the frictional bearing was selected at 0.02 based on the median design value of the code requirement (CRC 2013). The coefficient ( $\mu$ ) of the sliding surface between the bottom plate of the fixed bearing and the sand-cement mortar layer shown in Figure 5 was selected as 0.2, which

was obtained from the Cl. 6.2.2(6) of EN 1993-1-8 (CEN 2005). Hence, the Coulomb friction force ( $F_{max}$ ) for the frictional and fixed bearings was 122.8 kN and 1228 kN, respectively. In addition, the maximum static deformation ( $x_y$ ) of all the types of bearings was selected as 2 mm, which is the maximum allowable bearing deformation under the design loads (CRC 2013).



(a) EPP model for the sliding response of the bridge bearings

(b) Material model simulating the fixity of the fixed bearings

**Figure 10 Material properties for simulating bridge bearings**

Moreover, previous literature reviews show that the functionality of the HSR bridge is highly dependent on the damage occurring in the bearings, especially the fixed bearings in the MSSS bridge system. Hence, this thesis investigates the influence of different shear strengths of the fixed bearings on the seismic performance of the entire MSSS bridge system.

The total shear strength of the two fixed bearings at the left end of each girder was simulated using an additional zero-length spring element with the elastic material property, as shown in Table 10(b). Five levels of shear strength ( $F_{shear}$ ) were examined in this study, which are 0 kN, 1875 kN, 3750 kN, 5625 kN and 11200 kN, giving the base shear coefficients of 0, 0.15, 0.30, 0.45 and 0.90, respectively. It should be noted that these coefficients are calculated based on

the 5000 kN vertical design load ( $N_v$ ) per bearing multiplied by a safety factor of 1.25, as follows:

$$\frac{F_{shear}}{1.25N_v}$$

Furthermore, an element removal algorithm, first introduced by Talaat and Mosalam (2009) and further developed by Li (2014), is applied on this additional zero-length element. Hence, before fracture and sliding occur in the fixed bearings, the additional zero-length element with five levels of shear strength provides the fixity and transfers the seismic loads from the superstructure to the substructure of the bridge. When the internal force of this element first exceeds  $F_{shear}$  during the non-linear time-history analysis of the bridge model, the element will be removed and the other zero-length spring element of fixed bearing will begin to simulate the sliding response of the fractured fixed bearings. The procedures of the direct removal techniques are summarized in Figure 11 below.

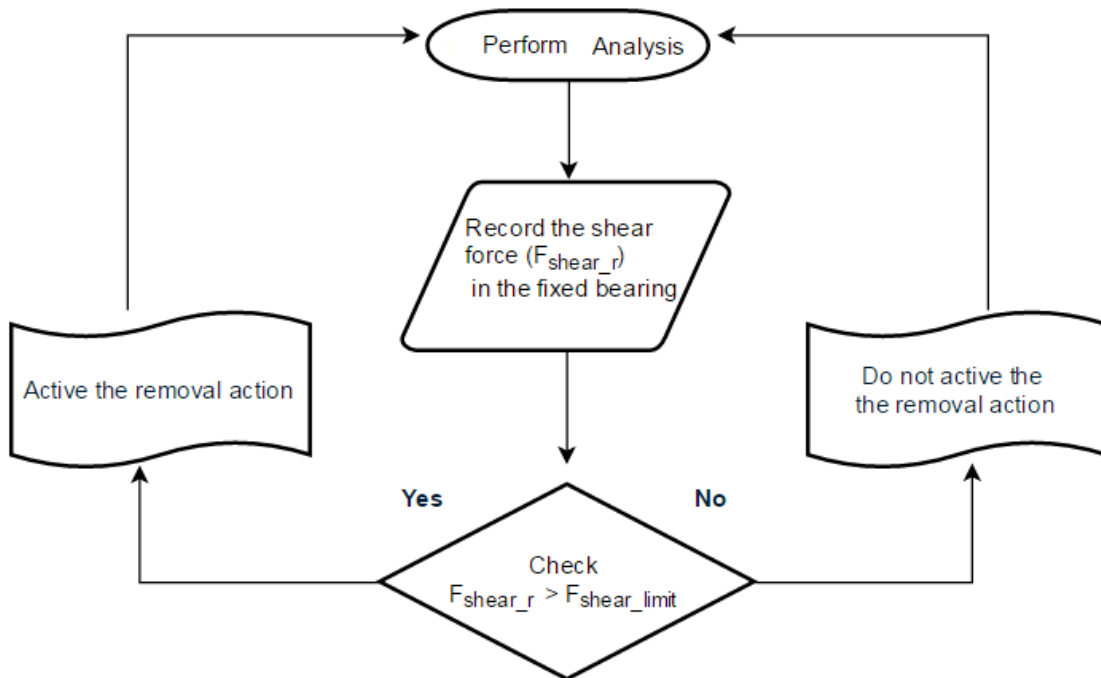


Figure 11 The procedures of direct element removal for each fixed bearing

### 3.1.3 The MSSS Bridge Girder and Joint Modeling

The 32-meter box girder was modeled using the elastic element, where the axial stiffness and bending stiffness were modeled using the property as presented in Figure 2. The total mass of each girder was modeled at 1250,000 kg. The mass was assigned as nodal masses ( $m_2$ ) and applied equally to all eight bearing supports on the girder.

The girder and abutment joint were modeled as truss elements with ElasticBilin material in OpenSees, where the force-deformation response was shown in Figure 12. The initial stiffness ( $k_1$ ) was calculated as  $2.5 \times 10^4$  kN/m, which was obtained from experimental investigation into the longitudinal stiffness of the CRTS II track-slab system (Sun 2011). The post yield stiffness ( $k_2$ ) equals to  $1.9 \times 10^6$  kN/m, which was obtained from a study of the longitudinally compressive stiffness of the box girder (Zhu 2013). The stiffness of the element was assumed to be linear until the girder gap of the joint shown in Figure 3(b) was closed. The gap ( $X_1$ ) between the two adjacent girders was 100 mm.

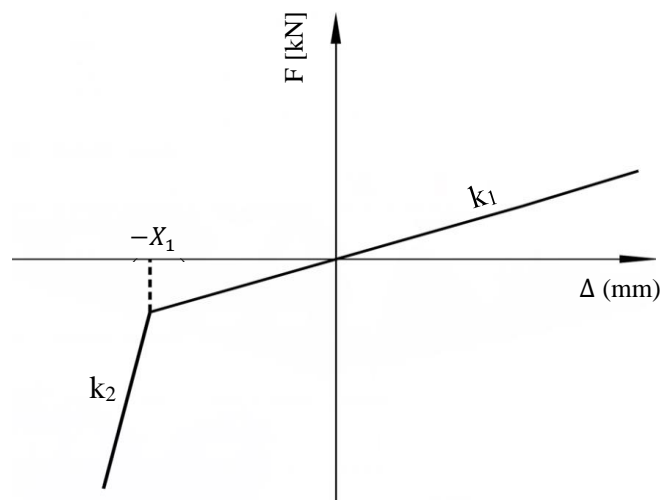


Figure 12 Material properties for the element of girder joints in OpenSees.

Table 1 illustrates the first four fundamental vibration periods of the typical four-spanned HSR MSSS bridge structure, which is obtained from an eigenvalue analysis of the bridge model in OpenSees.

**Table 1 Fundamental vibration periods of the typical four-span HSR MSSS bridge**

	<b>T1 (sec)</b>	<b>T2 (sec)</b>	<b>T3 (sec)</b>	<b>T4 (sec)</b>
<b>Bridge Model</b>	1.04	0.82	0.67	0.59

### 3.2 Seismicity and Ground Motion Selection

Figure 13 illustrates a seismic hazard map of China (Wu et al. 2017). The Sichuan-Yunnan region in Southwest China is in the Eastern Indo-Asian region, where the Tibetan Plateau and the South China Plain collide. Many highly active faults exist in this region, which impose highest level of seismic hazards in China according to the seismic hazard maps from the China Design Code. (CEA 2015). 12 severe earthquakes with magnitudes over  $M_w = 7.0$  have occurred in this region since 1970.

Two major HSR corridors are currently operating in this highly active earthquake zone. The Kunming – Shanghai HSR line is operating in the highest intensity (IX) region in Yunnan Province, China while the Chengdu – Xi’an HSR line closely passed through the hardest hit areas during the 2008 Wenchuan earthquake. In addition, multiple inter-city HSR lines will be completed in these highly active earthquake zone by the end of 2020.

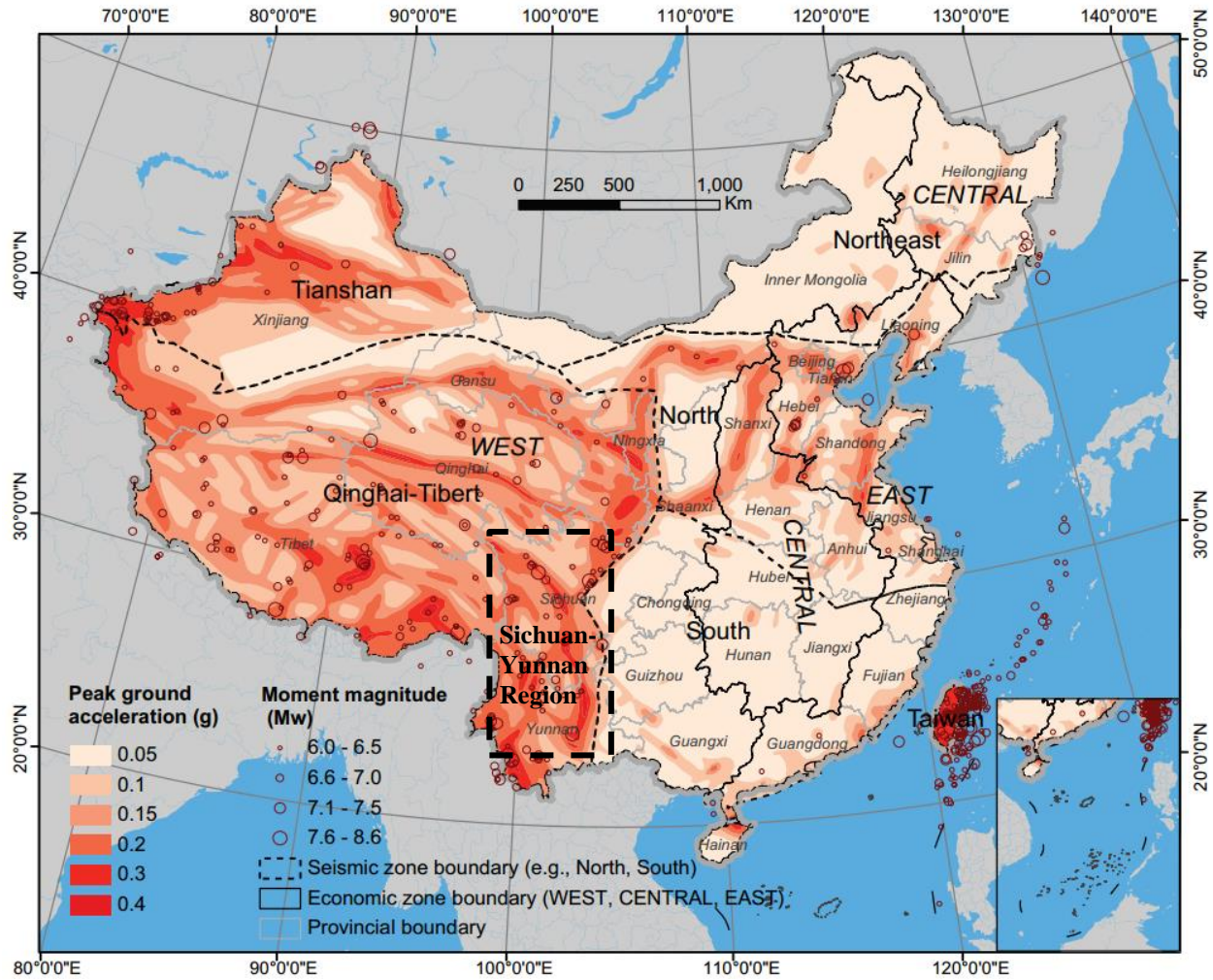
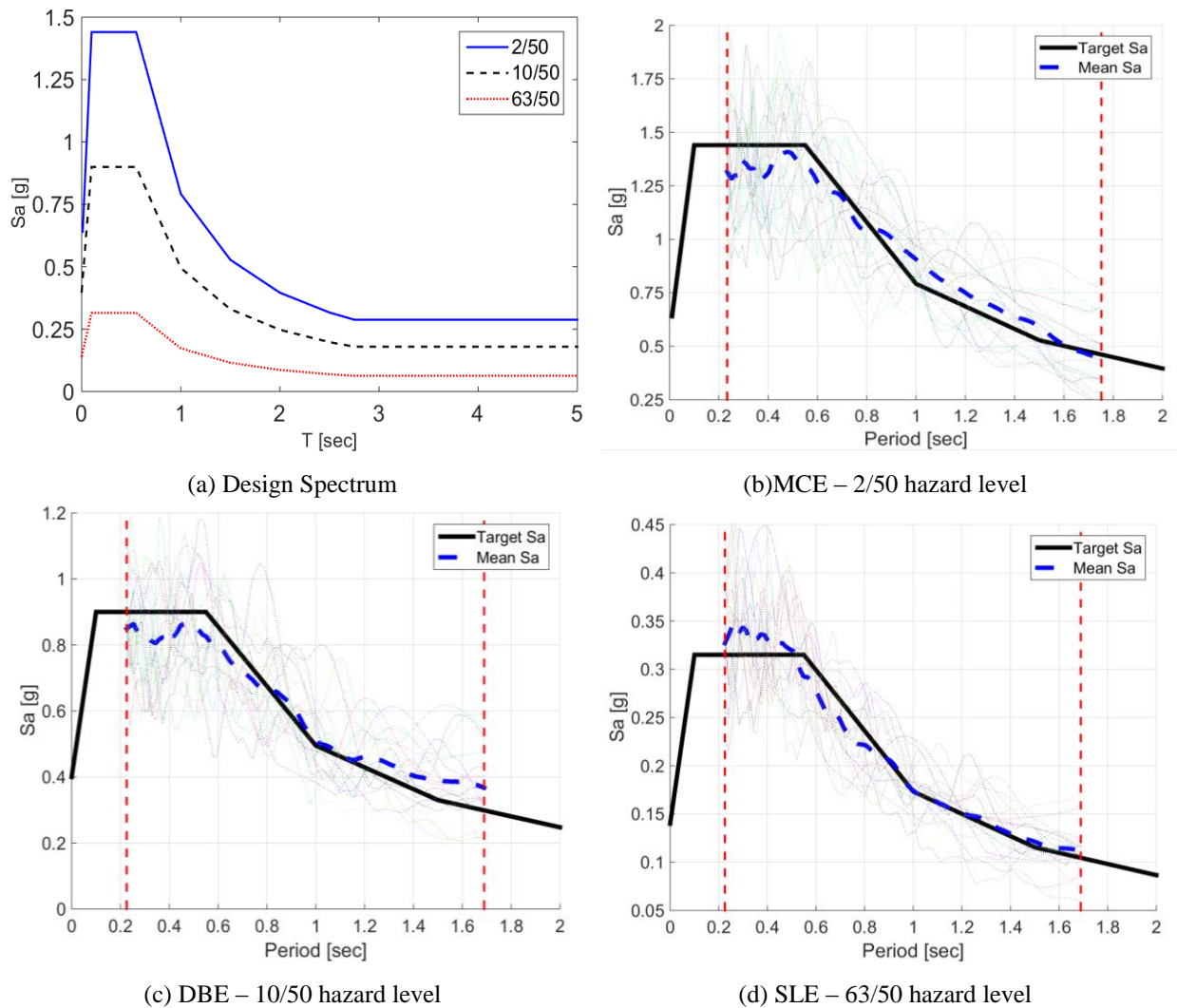


Figure 13 China's seismic hazard maps of the PGA zonation at 10% in 50 years (Permission from Wu et al. 2017)

Three seismic hazard levels which correspond to: a) Maximum Considered Earthquake (MCE): 2% probability of exceedance in 50 years (2/50); b) Design Based Earthquake (DBE): 10% probability of exceedance in 50 years (10/50); and c) Service Level Earthquake (SLE): 63% probability of exceedance in 50 years (63/50) were identified from the China Code for the Seismic Design of Railway Engineering (China CR 2006). Figure 14 shows the target spectra developed for this study. 18 ground motions with magnitudes between  $M_w = 6.5$  and  $M_w = 7.5$ , scale factors between 0.1 and 5, closest distances to fault within 100 km and shear wave velocities of soil at 30

meter below grade ( $V_{s30}$ ) between 150 m/s and 760 m/s were selected from PEER NGA-west 2 database (Ancheta et al. 2014). The ground motions were amplitude scaled such that the scaled spectra over the period range from  $0.2 T_1$  to  $1.5 T_1$  ( $T_1 = 1.126$  sec is the fundamental period of a four-span HSR MSSS bridge) match the target spectrum. This scaling procedure is consistent with the scaling procedure as outlined in ASCE 7-16 provisions (ASCE 2010). Figure 14 (b) to 7 (d) shows the scaled spectra on top of the target spectrum.



**Figure 14 Design spectrum and ground motions for each hazard level**



### 3.3 Seismic Responses of the Four-Span HSR MSSS Bridge Model

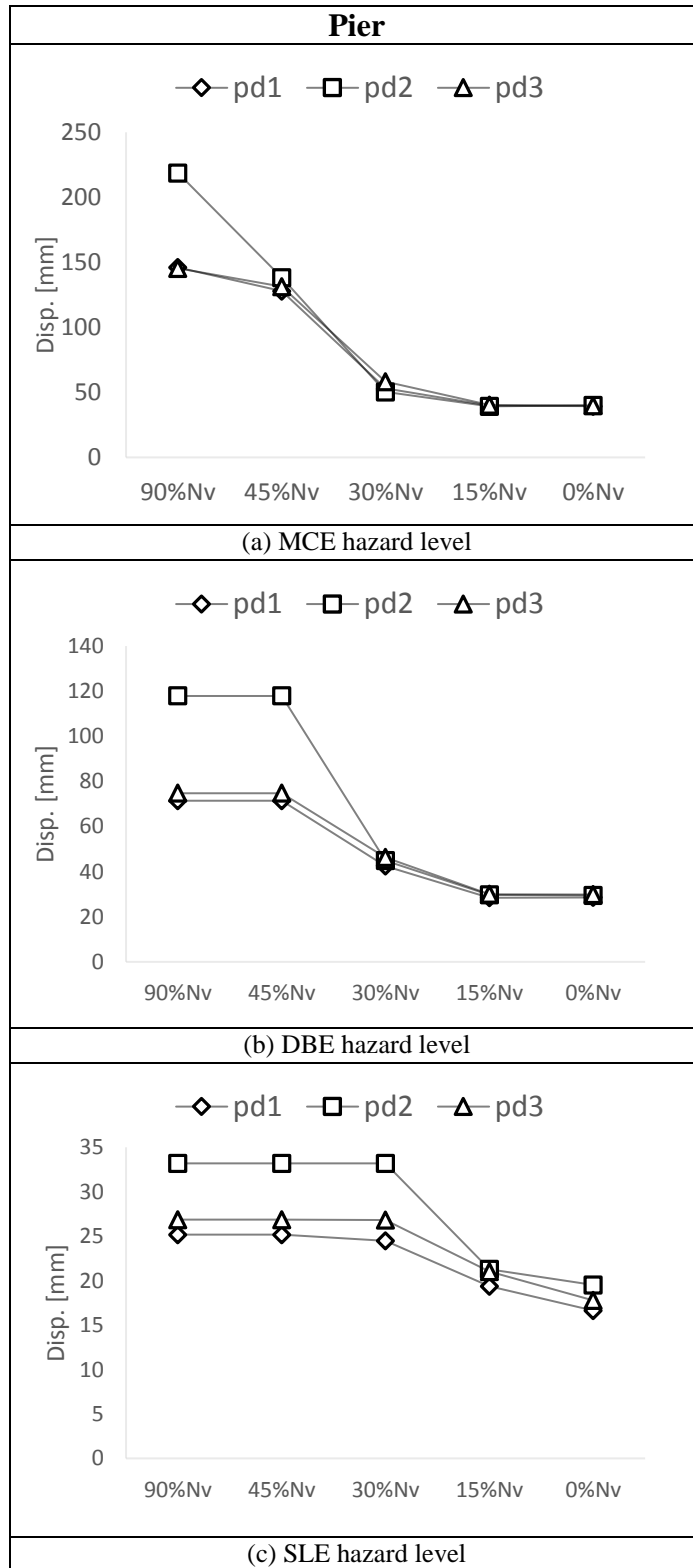
The median peak displacement of the bridge piers, bridge bearings and bridge girder joints from the 18 ground motions were summarized in Figure 15, Figure 16 and Figure 17, respectively.

As presented in Figure 15 (a), (b) and (c), the middle pier (pd2) of the bridge produced the highest drift under all hazard levels considered. The results also show that the pier drift decreases significantly when the shear strength of the fixed bearing exceeds  $30\% N_v$ .

As presented in Figure 16 (a), (b) and (c), The fixed bearings (df3) at the top of the middle pier has the highest displacement in all cases. In addition, the three plots show shear strength has limited impacts on the relative displacement of the bearings once the fixed bearing is fractured. As presented in Figure 16 (d), (e) and (f), the seismic responses of sliding bearings are stable until the fixed bearings are fractured. After the fixed bearing lost its restraint, the seismic responses of both type of bearings have demonstrated a similar trend.

As presented in Figure 17 (d), the 3<sup>rd</sup> girder joint (dgc3) produced the largest seismic responses. At the MCE level, the 3<sup>rd</sup> girder joint experienced pounding effects at all cases. At the DBE level, the displacement of girder joint decreases as the shear strength of fixed bearings decreases.





**Figure 15 Median peak drift developed at piers**

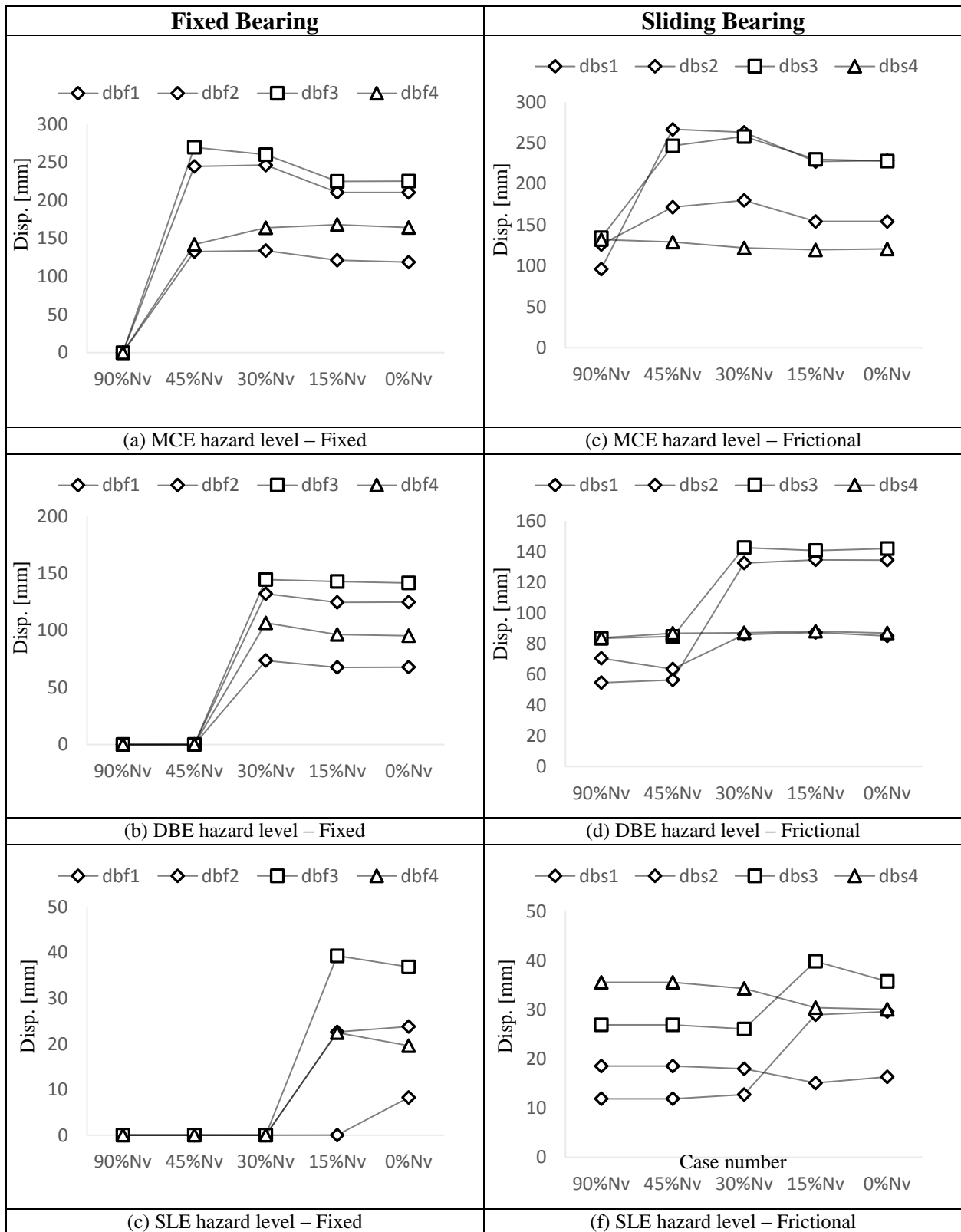


Figure 16 Median peak longitudinal relative displacement developed at bearings

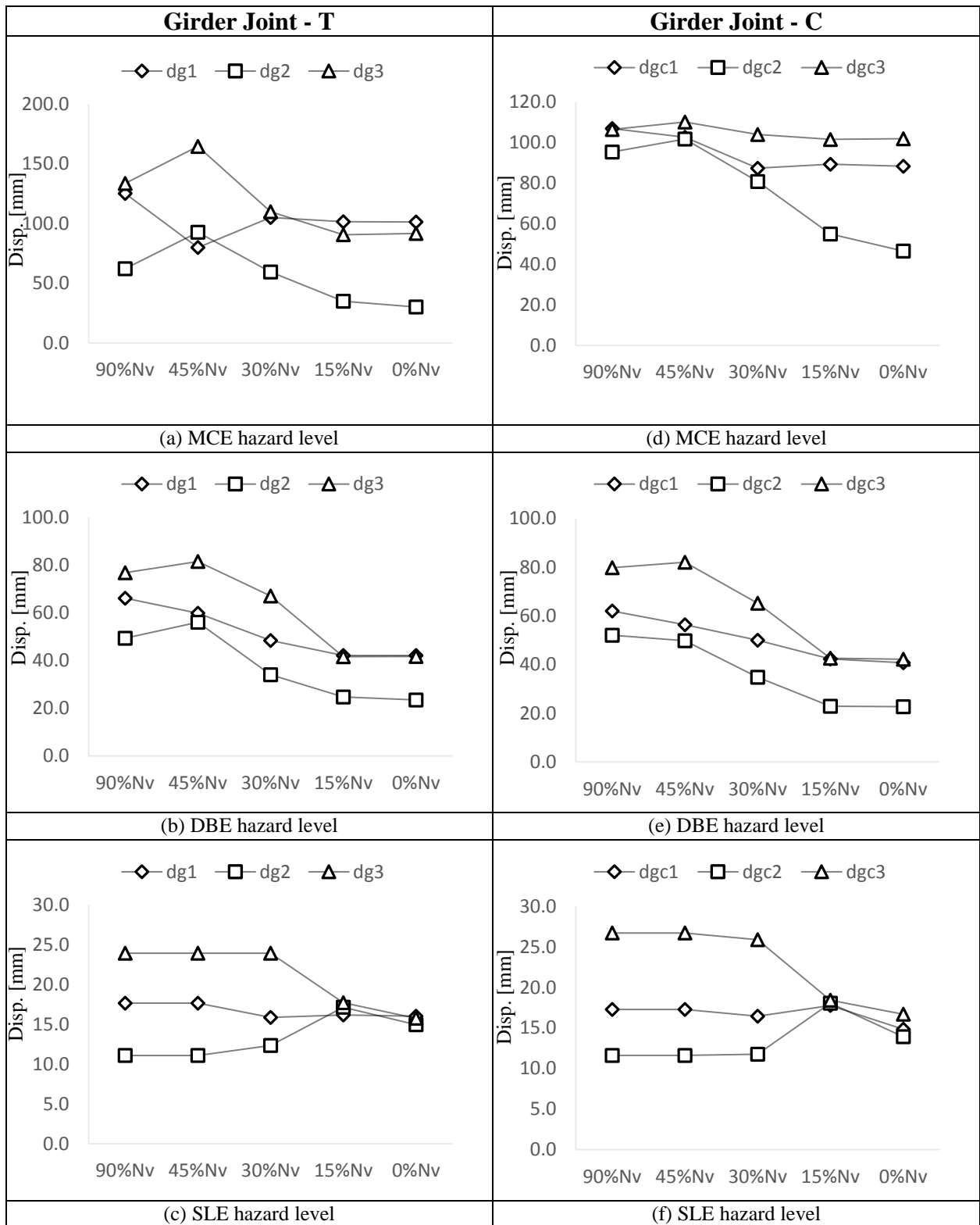


Figure 17 Median peak tensile and compressive displacement developed at girder joints

### **3.4 Summary**

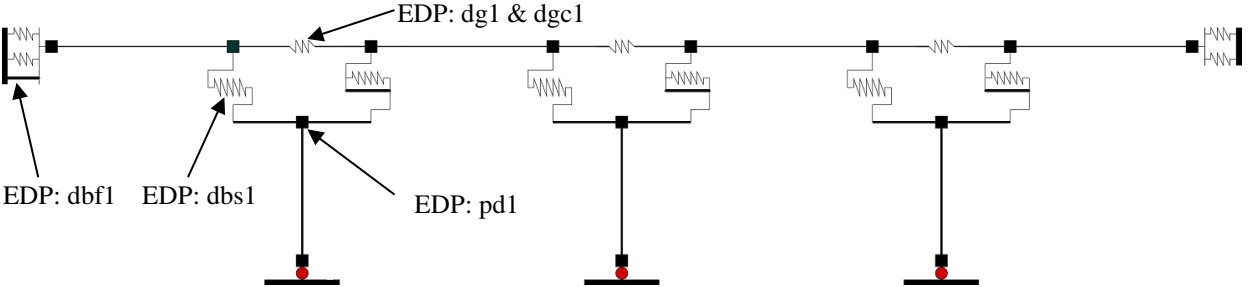
The longitudinal seismic response of a typical four-span HSR MSSS bridge was effectively simulated in OpenSees. The bridge models with fixed bearings at five different levels of shear strength were constructed. An element direct removal technique was applied to simulate the fracture and sliding response of the fixed bearings. In addition, the seismic hazard of southwest China, the Yunnan-Sichuan region, was investigated. 18 ground motions were selected and scaled to the three hazard levels of the target spectrum. Then, the response analysis of this bridge system was conducted using the non-linear time-history analysis in OpenSees. The simulated seismic response of each bridge component under selected ground motions will be used to quantify the corresponding seismic damages, and to further conduct the seismic performance evaluations outlined in the subsequent chapter.

# Chapter 4: The Performance-based Methodology for Evaluating the Multi-Span Simply Supported Bridge Response

The purpose of this chapter is to evaluate the seismic performance of the typical HSR MSSS bridge through calculating the expected monetary loss under the three hazard levels. A thorough damage state and repair actions analysis of the bridge's key components were conducted. The final results of this performance-based evaluation were presented in terms of the Total Structural Repair (TSR) costs and Total Travel Delay (TTD) costs, which were calculated based on the PBEE framework outlined presented in this chapter. The influence of the different shear strength of the fixed bearings on the seismic performance of the bridge was thoroughly investigated.

## 4.1 Performance Groups

A total of 21 performance groups of the prototype HSR MSSS bridge was identified. These components can be classified into five categories of performance groups (PG): 1) Bridge piers; 2) Fixed bearings; 3) Frictional bearings; 4) Track-slab system, and 5) the continuous roadbed system included in this study. Table 2 lists these performance groups and their corresponding EDPs. The location of each EDP is illustrated in Figure 18.



**Figure 18 The location of each type of EDPs of the 21 PGs of the typical four-span HSR MSSS bridge**

**Table 2 Summary of performance groups**

PG No.	PG Name	EDP	EDP Description	PG Description
1	SP1	pd1	Peak drift at top of Pier 1 [mm]	Bridge Piers
2	SP2	pd2	Peak drift at top of Pier 2 [mm]	
3	SP3	pd3	Peak drift at top of Pier 3 [mm]	
4	FB1	dbf1	Peak displacement at fixed bearing 1 [mm]	Fixed Bearings
5	FB2	dbf2	Peak displacement at fixed bearing 2 [mm]	
6	FB3	dbf3	Peak displacement at fixed bearing 3 [mm]	
7	FB4	dbf4	Peak displacement at fixed bearing 4 [mm]	
8	SB1	dbs1	Peak displacement at frictional bearing 1 [mm]	Frictional Bearings
9	SB2	dbs2	Peak displacement at frictional bearing 2 [mm]	
10	SB3	dbs3	Peak displacement at frictional bearing 3 [mm]	
11	SB4	dbs4	Peak displacement at frictional bearing 4 [mm]	
12	CR1	dbf1	Vertical settlement at track-slab segment 1 [mm]	Track-Slab System
13	CR2	dbf2	Vertical settlement at track-slab segment 2 [mm]	
14	CR3	dbf3	Vertical settlement at track-slab segment 3 [mm]	
15	CR4	dbf4	Vertical settlement at track-slab segment 4 [mm]	
16	BS1	dg1	Peak expansion at girder joint 1 [mm]	Roadbed - Tensile Failure
17	BS2	dg2	Peak expansion at girder joint 2 [mm]	
18	BS3	dg3	Peak expansion at girder joint 3 [mm]	
19	BC1	dgc1	Peak contraction at girder joint 1 [mm]	Roadbed – Compressive Failure
20	BC2	dgc2	Peak contraction at girder joint 2 [mm]	
21	BC3	dgc3	Peak contraction at girder joint 3 [mm]	

## 4.2 Damage and Loss Analysis

Distinct damage states (DSs) were defined for each of the PG. The DSs were defined based on the peak Engineering Demanding Parameter (EDP), such as peak drift or bearing displacement. In each of the DS, the repair method and downtime were defined. This data was obtained from a detailed literature review of actual engineering documents (Yu 2015 and Ran 2009). The results were presented using continuum fragility curves.

Total Structural Repair (TSR) costs and Total Travel Delay (TTD) costs were chosen as the decision variables. The TSR represents the direct costs related to structural repair while the

TTD represents the indirect costs associated with the loss in revenue due to the train being unable to operate as a result of repair efforts. In most cases, the TTD outweighs the TSR. To calculate the TTD costs, a repair method was first selected for each DS within each PG. Next, the TTD duration was summed up for all PGs. The final TTD costs were then calculated using the average daily revenue (ADR) of the HSR line multiplied by the TTD duration. The ADR of the Leshan-Jiangyou HSR line was estimated to be 2.4 million RMB (SCED 2017). It should be noted that this is a conservative estimate of the ADR value, since the traffic for the HSR is expanding rapidly in this region, and daily ridership is expected to expand significantly when new railway lines start to operate in this region by the end of 2020. It should be noted that not all PGs contribute to the TTD costs. This is because the repair method for these PG, which may involve installing circular steel jackets for HSR MSSS bridge piers, will not affect the HSR operation. Table 3 provides a summary of repair methods and their corresponding TTD durations.

**Table 3 Repair methods and corresponding bridge closure times**

<b>Bridge components</b>	<b>Repair method</b>	<b>Downtime</b>
Piers PG	1) seal cracks and minor patching of concrete	0 days
	2) seal cracks and major patch of concrete	0 days
	3) replacing column with temporary support	1 day
Bearing PG	1) rebuild the supporting mortar layer for bearing	4 hours/pair
	2) replace bearing by jacking up girders	4 hours/pair
	3) longitudinal restoring of girder position	4 hours/girder
Roadbed PG	1) seal cracks and patching of concrete	0-1 days/span
	2) rebuild by cast-in-place	10 days/span
Track-Slab PG	1) seal cracks	0
	2) replace slab and calibrate rail	3 days/span
	3) replace the whole track-slab and calibrate rail	15 days/span
Bridge Girder	Rebuild superstructure due to global collapse	45 days/span


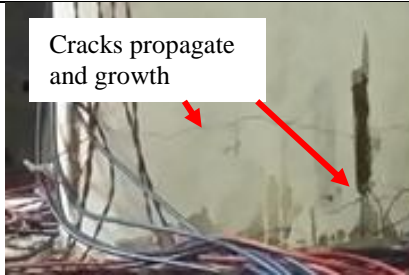
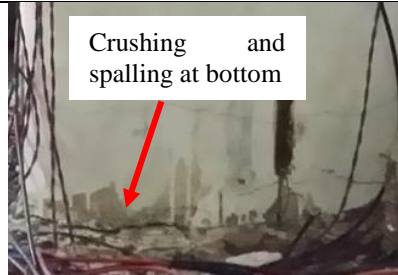
The TSR costs were calculated using the total repair quantities multiplied by the unit repair costs. In actual engineering projects, the unit repair cost usually decreases as the total quantity

increases. In this study, the Average Unit Cost (AUC) was first calculated based on the average construction cost of a 20-km segment of the HSR MSSS bridge (Sun, 2008). The unit repair cost begins at three times the AUC. When the repair quantity exceeds the quantities in a 20-km segment of the HSR MSSS bridge, the unit repair cost decrease to the save amount as the AUC. Any intermediate quantity is linearly interpolated.

#### 4.2.1 HSR MSSS Bridge Pier Performance Groups

The peak drift ratio of the HSR MSSS bridge pier was selected as the EDP to quantify the seismic performance of the pier group. Four DSs were defined for the HSR MSSS pier. These DSs include: DS1) No damage, DS2) Moderate cracking, DS3) Degradation without failure, and DS4) Failure with crushing and spalling. The median EDP limit of each DS is defined based on the data obtained from the tests conducted by Jiang et al. (2013), shown in Table 4. To account for the uncertainty, the dispersion ( $\beta$ ) value of 0.4 was selected. This dispersion value was adopted based on the uncertainty presented in the FEMA P-58-1 document (FEMA 2012). The DSs and the associated repair quantity and unit repair cost for the HSR MSSS bridge are presented in Table 4 and Table 5, respectively (Xu 2010).

**Table 4 Damage states of HSSS HSR pier (obtained from Jiang et al. 2013)**

DS2	DS3	DS4
		
Drift Ratio (EDP) = 0.3%	Drift Ratio (EDP) = 2.0%	Drift Ratio (EDP) = 2.4%



**Table 5 Repair quantities and unit costs for the pier PG**

Repair actions	Pier			Unit cost [ $10^4$ RMB]			
	DS2	DS3	DS4	Min. Qty.	Max. Qty.	Max. cost	Min. cost
Pier repair	0.10	0.5	1	1	600	165	55
Downtime [days]	0	0	1	1	1000	240	240

#### 4.2.2 Bearing Performance Groups

The peak relative displacement between the girder and pier-top was selected as the EDP to quantify the DS for the fixed and frictional bearing PGs. Three DSs were defined for the bearing PGs. These DSs included: DS1) No damage, DS2) Bearing damage due to exceeding the service limit state (SLS) of deformation, and DS3) Unseating failure of the bearing. The median EDPs were employed to define the DSs of the bearing PGs obtained from the design code (CRC 2013) and from the engineering design drawings of the TJQZ-8360 steel spherical bearings. Table 6 shows the DS threshold values of the fixed and frictional bearing PGs. The dispersion value of the bearing PGs was reduced from 0.4 to 0.25 since the uncertainties associated with the dimensions of each standard component of this PG were relatively small.

**Table 6 Damage states and fragility curves for fixed and sliding bearing**

Fixed bearing PGs				Frictional bearing PGs			
<i>DS</i>	<i>EDP</i>	$\beta$	<i>Description of DS</i>	<i>DS</i>	<i>EDP</i>	$\beta$	<i>Description of DS</i>
>DS2	2 mm	0.25	SLS of deformation	>DS2	60 mm	0.25	SLS of sliding distance
>DS3	600mm	0.25	Unseating failure	>DS3	220mm	0.25	Unseating failure
(a) Damage states of fixed bearing PGs				(b) Damage states of sliding bearing PGs			
(c) Damage states of fixed bearing PGs				(d) Damage states of frictional bearing PGs			

Table 7 presents a summary of the repair quantities and unit repair costs of the bearing performance group obtained from Shen et al. (2012). The unit cost related to restoring girder position was directly calculated based on the method proposed by Shen et al. (2012), which does not require adjustment for low quantities of repair actions.

**Table 7 Repair quantities and unit costs for bearing PGs**

Repair Actions	Fixed bearing		Frictional bearing		Unit Cost [ $10^4$ RMB]			
	DS2	DS3	DS2	DS3	Min. Qty.	Max. Qty.	Max. cost	Min. cost
Replacing bearing plates	2	0	2	0	1	2000	1.5	0.5
Replacing the entire bearings	0	2	0	2	1	2000	3	1
Jacking up of girder	1	2	1	2	1	1000	15.4	15.4
Restoring girder positions (long.)	1	2	1	2	1	1000	5.0	5.0
Downtime (days)	0.5	1	0.5	1	1	1000	240	240

### 4.2.3 Track-slab Performance Group

The identical peak relative displacement between the girder and pier-top selected as the EDP to quantify the DS for the track-slab PG. Four DSs were defined for track-slab PGs. These included: DS1) No damage, DS2) Vertical settlement of the girder due to the frictional bearing unseating failure, DS3) Vertical settlement of the girder due to the fixed bearing unseating failure, and DS4) Global collapse due to girder unseating failure. Table 8 displays the median damage threshold value for the track-slab PGs for each DSs. Table 9 reveals the repair quantity and unit repair costs of the track-slab PGs. The average construction costs (min. cost) of the slab and track of the CRTS II system were obtained from Liu (2015) and Jiang (2015). It should be noted that the vertical displacement caused by bearing unseating failure (DS3) was assumed to impact the track-slab system in the vicinity of the pier-end. The seismic performance of the track-slab system, which rests on the centre of the girders, was assumed to relate to the longitudinal movement of the continuous roadbed PG.

**Table 8 Median EDP and dispersion ( $\beta$ ) values for reaching each DS of the track-slab PGs**

PG	>DS2		>DS3		>DS4	
	EDP[mm]	$\beta$	EDP[mm]	$\beta$	EDP[mm]	$\beta$
Track-Slab	220	0.25	600	0.25	1450	0.25

**Table 9 Repair quantities and unit costs of the track-slab PGs**

Repair Actions	Track-slab PG			Unit Cost [ $10^4$ RMB]			
	DS2	DS3	DS4	Min. Qty.	Max. Qty.	Max. cost	Min. cost
Slab repair	0.3	0.5	1	1	600	117	39
Track (CW rail) repair	0.5	0.5	1	1	600	108	36
Downtime (days)	3	15	45	1	1000	240	240

#### 4.2.4 Roadbed Performance Group

The median peak longitudinal displacement developed in the girder joint elements was selected as EDPs used for measuring the seismic performance of the roadbed PGs. Since the seismic damage of the two PGs caused by the closure and expansion of the girder joints was different, the peak tensile displacement (expansion) and peak compressive displacement (contraction) of the girder joints were used to measure separately the two types of damage.

The continuous roadbed is made of RC concrete, so the four DSs were defined for the roadbed PGs. These included: DS1) No damage, DS2) Cracking, DS3) Degradation without failure, and DS4) Failure. The strain limits of each DS are summarized in Table 10, and were obtained from the Chinese concrete design code (China MOHURD 2010) for C30 concrete with HRB500 steel. The corresponding EDPs were calculated by multiplying the strain ratio by 32.7 meters. This is the length between the two groups of shear studs connecting the roadbed with its support girders, illustrated in Figure 3(b) and (c). The dispersion values of each DS selected at 0.4 accounted for the uncertainties in the concrete and steel materials.

**Table 10 Median EDP value for reach each DS of the roadbed PGs**

Roadbed PG	Roadbed (Tensile)			Roadbed (Compressive)		
	DS2	DS3	DS4	DS2	DS3	DS4
<b>Strain</b>	0.02%	0.2%	4%	0.074%	0.2%	0.35%
<b>EDP [mm]</b>	6.5	65	1308	24	65	114
<b>Dispersion (<math>\beta</math>)</b>	0.4	0.4	0.4	0.4	0.4	0.4

The repair quantities and costs for the tensile and compressive DSs are summarized in Table 11. The compressive DSs developed in the roadbed directly affected its flatness level as well as the alignment of the track-slab PGs. Hence, the repair quantities were assigned to both roadbed and track-slab PGs. Meanwhile, the alignment of the track-slab PGs will not be affected by the

tensile DSs of the roadbed PGs because the connection (the CA mortar layer) between the two PGs is weak. When a large tensile displacement developed in the roadbed, the fractured CA layer is assumed to isolate the excessive displacement on its supporting structures. Moreover, the performance of the roadbed PG is measured based on the value of the two EDPs. Hence, up to 50 percent of the original construction costs of the PG were assigned to their DS4.

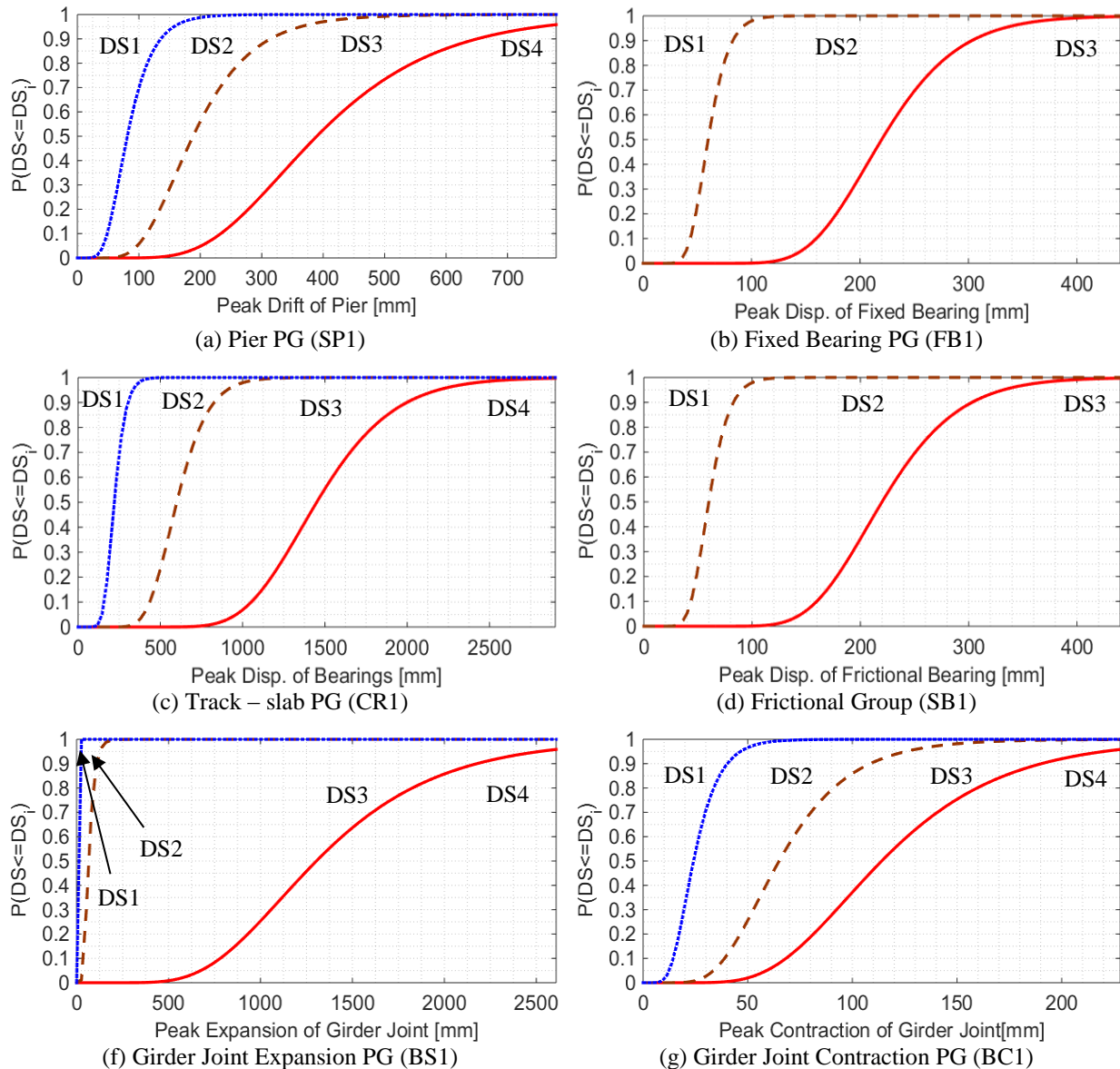
The AUC and repair time were estimated based on the construction manual of the Shanghai-Kunming HSR line. It should be noted that the major part of the downtime was used to calibrate the alignment of the tracks rather than to repair the cracks in the roadbed.

**Table 11 Repair quantities and unit costs of roadbed PGs**

Repair Actions	Roadbed (Tensile failure)			Roadbed (Comp. failure)			Unit Cost [ $10^4$ RMB]			
	DS2	DS3	DS4	DS2	DS3	DS4	Min. Qty.	Max. Qty.	Max. cost	Min. cost
Slab repair				0	0.1	0.5	1	600	117	39
Track repair				0	0.1	0.5	1	600	108	36
Roadbed repair	0.1	0.25	0.5	0.1	0.25	0.5	1	600	29.25	9.75
Downtime (days)	0	1	10	0	1	10	1	1000	240	240

#### 4.2.5 Damage Fragility Curves

Based on the above fragility data, the fragility curves of each PG were developed and are displayed in Figure 19. By using the PBEE methodology outlined in the FEMA P-58-1 (FEMA 2012), rigorous seismic performance-based evaluation could be conducted for each case of the four-span HSR MSSS bridge models.



**Figure 19 Damage fragility curves for each PG of the prototype bridge model**

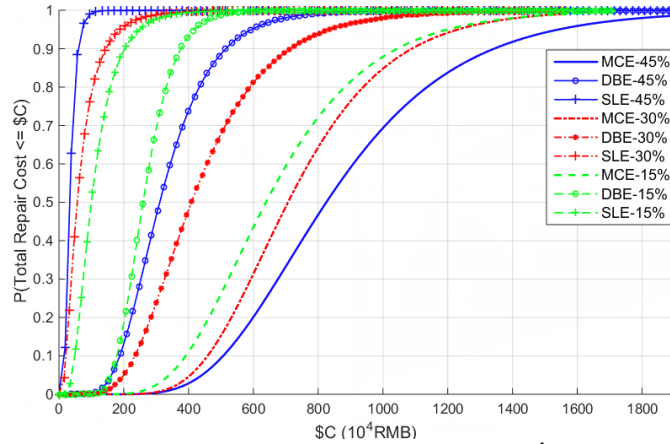
### 4.3 Seismic Performance Evaluation

Figure 8 illustrates the performances of a four-span HSR MSSS bridge under three seismic shaking intensities (SLE (63% in 50 years), DBE (10% in 50 years) and MCE (2% in 50 years)) were studied. As discussed in Chapter 3.1.2, five levels of shear strength (0 kN (0%  $N_v$ ), 1875 kN (15%  $N_v$ ), 3750 kN (30%  $N_v$ ), 5600 kN (45%  $N_v$ ) and 11200 kN (90%  $N_v$ )) for the fixed bearings

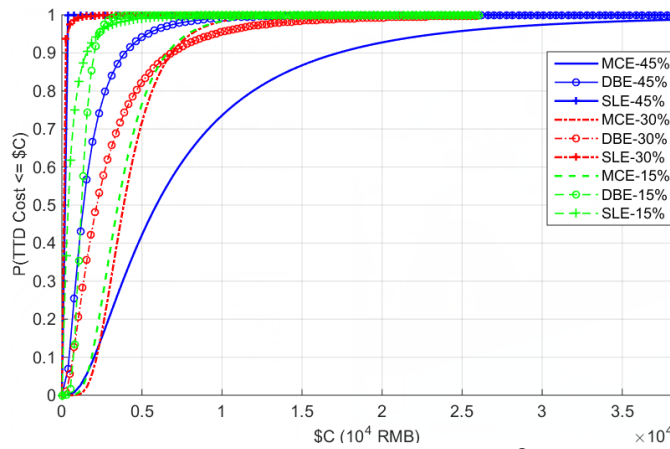
were studied. It should be noted that the longitudinal uncracking strength of piers is 4900 kN, which is between 30%N and 45%N. Hence, if the bearing shear capacities are less than 3750 kN ( $30\%N_v$ ), then the failure of the bearing is expected to occur before the pier cracks. On the other hand, if the bearing shear capacities are greater than 45%N, the pier is expected to crack before the fixed bearings fail in shear.

#### **4.3.1 The Cumulative Distribution Function of TSR and TTD costs**

Figure 20 (a) and (b) shows the cumulative distribution function (CDF) for the TSR costs and TTD costs under the three hazard levels considered. At each hazard level, the performance of the bridge with fixed bearings at three shear design capacities 1875 kN ( $15\%N_v$ ), 3750 kN ( $30\%N_v$ ), 5600 kN ( $45\%N_v$ )) were evaluated. The median costs are summarized in Table 12. As presented in Table 12, for the  $45\%N_v$  case at the MCE hazard level, the median TTD cost is 7.15 times the TSR costs. At the MCE and DBE hazard level, the  $15\%N_v$  case has the lowest TTD and TSR costs. However, at the SLE hazard level, the  $15\%N_v$  case incurred the highest median costs. At the SLE hazard level, the TTD costs jumped from 1.39 to 4.03 million RMB when the shear capacity decreased from 3750 kN ( $30\%N_v$ ) to 1875 kN ( $15\%N_v$ ). This means decreasing the shear capacity of the fixed bearings will significantly increase the TTD costs and TML at the SLE level. Even though TSR and TTD costs under MCE and DBE levels can be reduced by using bearings with low shear capacity, the savings might be not enough to compensate for the increased costs associated with frequent earthquakes at the SLE hazard level. In addition, the  $45\%N_v$ ,  $30\%N_v$  and  $15\%N_v$  cases incurred the highest median costs at MCE, DBE and SLE level respectively. To determine the reasons that cause a higher seismic loss in each of these three cases, each CDF of TSR and TTD presented in Figure 20 was de-aggregated into the 21 PGs in the following section.



(a) Total Structural Repair (TSR) costs [ $10^4$ RMB]



(b) Total Travel Delay (TTD) costs [ $10^8$ RMB]

Figure 20 Cumulative distribution function of total monetary loss

Table 12 Median CDF cost of each case

Cases	MCE [Million RMB]		DBE [Million RMB]		SLE [Million RMB]	
	TSR	TTD	TSR	TTD	TSR	TTD
45% $N_v$	<b>8.25</b>	<b>59.04</b>	3.11	13.55	0.33	1.93
30% $N_v$	7.07	38.62	<b>4.09</b>	<b>21.85</b>	0.57	1.39
15% $N_v$	6.39	35.03	2.56	12.27	<b>1.00</b>	<b>4.03</b>

### 4.3.2 The De-aggregation of the TSR and TTD Costs

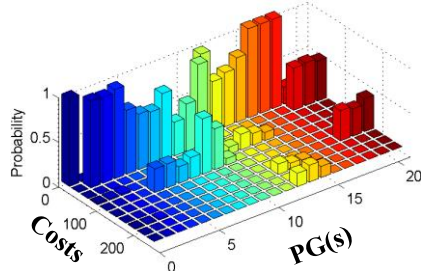
Figure 21 and Figure 22 illustrates the de-aggregation of TSR and TTD costs of the bridge model at three design levels of shear strength: 1875 kN ( $15\% N_v$ ), 3750 kN ( $30\% N_v$ ), 5625 kN ( $45\% N_v$ ), respectively. The distribution of costs is very similar for 45%, 30% and 15% cases.



However, at the MCE level, the 45%  $N_v$  case has an additional repair cost from PG 13 to 15. Similarly, the 30%  $N_v$  case at the DBE hazard level and the 15%  $N_v$  case at the SLE level also have additional repair costs from PG 13 to 15. Since the seismic performance of the track-slab system is directly related to damages occurring in bearing PGs, the seismic performance of the entire bridge system can be effectively improved by minimizing the damages developed in bearing PG under any hazard levels of ground motions.

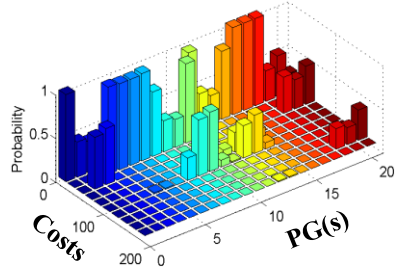
Another trend that can be observed from Figure 21 and Figure 22 is the TSR and TTD costs incurred by PG 19 to 21 at MCE level were slightly reduced by increasing the shear strength of fixed bearings. This type of seismic loss is still a large contribution to the TML of the bridge system, where the loss cannot be effectively reduced by shifting shear strength. In order to minimize this type of loss, the peak contraction of girder joints (PG 19 to 21) needs to be minimized.

Case: 5625 kN (45%) [ $10^4$ RMB]



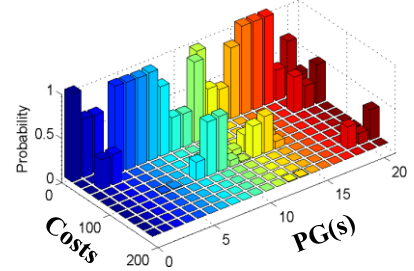
(a) MCE (2% in 50 years)

Case: 3750 kN (30%) [ $10^4$ RMB]

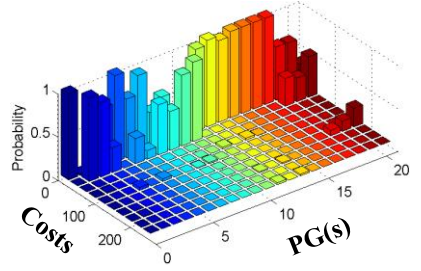


(d) MCE (2% in 50 years)

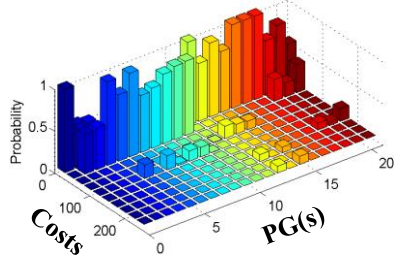
Case: 1875 kN (15%) [ $10^4$ RMB]



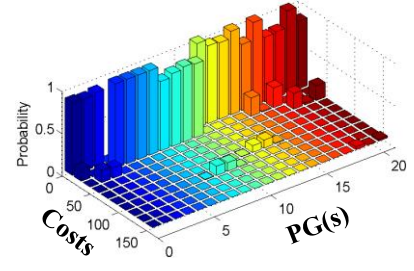
(g) MCE (2% in 50 years)



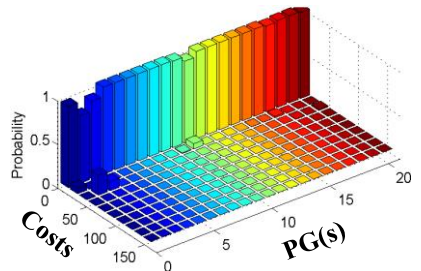
(b) DBE (10% in 50 years)



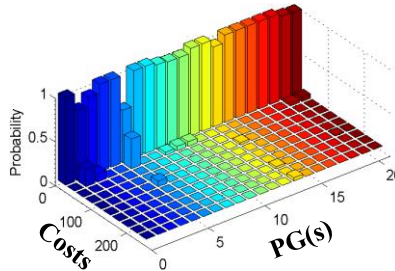
(e) DBE (10% in 50 years)



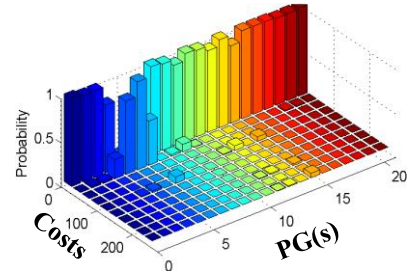
(h) DBE (10% in 50 years)



(c) SLE (63% in 50 years)



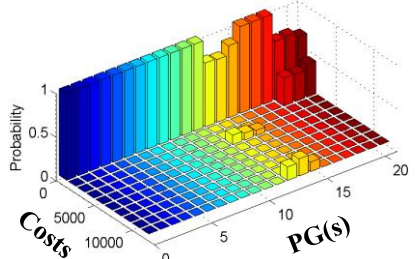
(f) SLE (63% in 50 years)



(i) SLE (63% in 50 years)

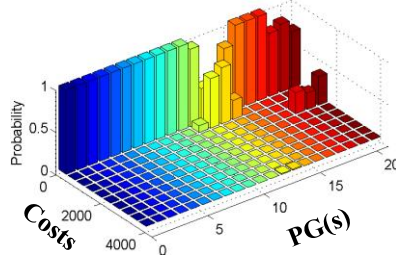
Figure 21 De-aggregation of TSR cost for each performance group

Case: 5625 kN (45%) [ $10^4$ RMB]



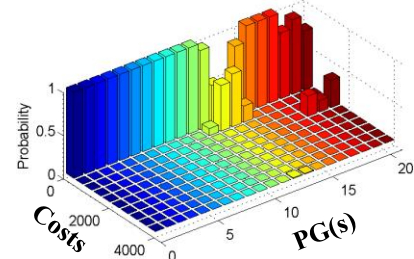
(a) MCE (2% in 50 years)

Case: 3750 kN (30%) [ $10^4$ RMB]

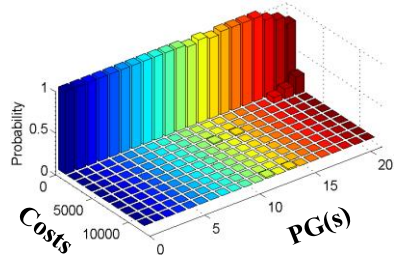


(d) MCE (2% in 50 years)

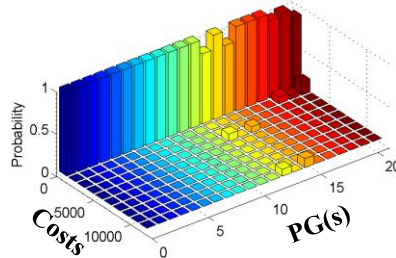
Case: 1875 kN (15%) [ $10^4$ RMB]



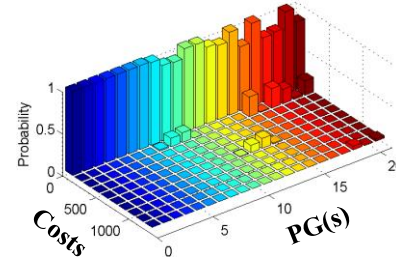
(g) MCE (2% in 50 years)



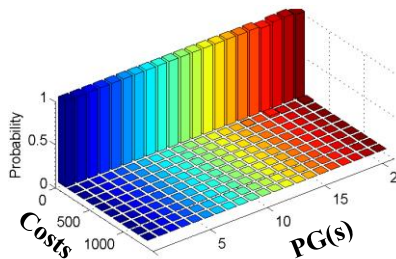
(b) DBE (10% in 50 years)



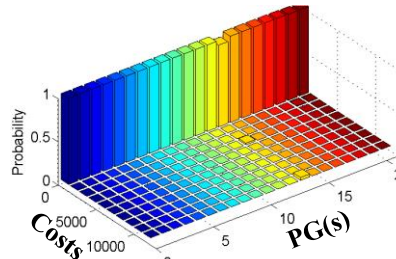
(e) DBE (10% in 50 years)



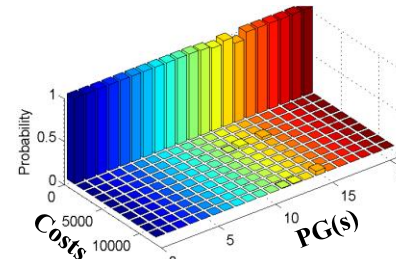
(h) DBE (10% in 50 years)



(c) SLE (63% in 50 years)



(f) SLE (63% in 50 years)



(i) SLE (63% in 50 years)

Figure 22 De-aggregation of TTD cost for each performance group

### 4.3.3 Time-based Assessments

To evaluate the seismic loss of the bridge system caused by all hazard levels of ground motions, the loss curves of TSR costs and TTD costs were developed for each case of the bridge model, as shown in Figure 23. The loss curve demonstrates the total loss as a function of the Annual Rate of Exceedance (ARE), and this total loss ( $\$C [10^4\text{RMB}]$ ) is plotted logarithmically. Figure 23 (a) and (b) both show that, at the same level of ARE, the total losses of  $45\%N_v$  and  $90\%N_v$

cases are significantly lower than that of the  $0\%N_v$ ,  $15\%N_v$ , and  $30\%N_v$ . In addition, the loss curves of  $45\%N_v$  and  $90\%N_v$  cases are very closely aligned.

As well, the Mean Annual Total Value of Loss (MAL) of each case was listed in Figure 23. By comparing the MAL in each case, it is evident the bridge model with the lowest shear strength produced the highest MAL. This contradicts the results presented in Table 12, since the rate of return on the SLE hazard level is much higher than those of other two hazard levels.

The listed MAL also demonstrates that using fixed bearings with shear strengths that are greater than 4900 kN (uncracking strength of pier) will significantly improve the overall seismic performance of the bridge. However, further increasing the shear strength of the fixed bearings will not lead to significant increases in the seismic performance of the bridge system.

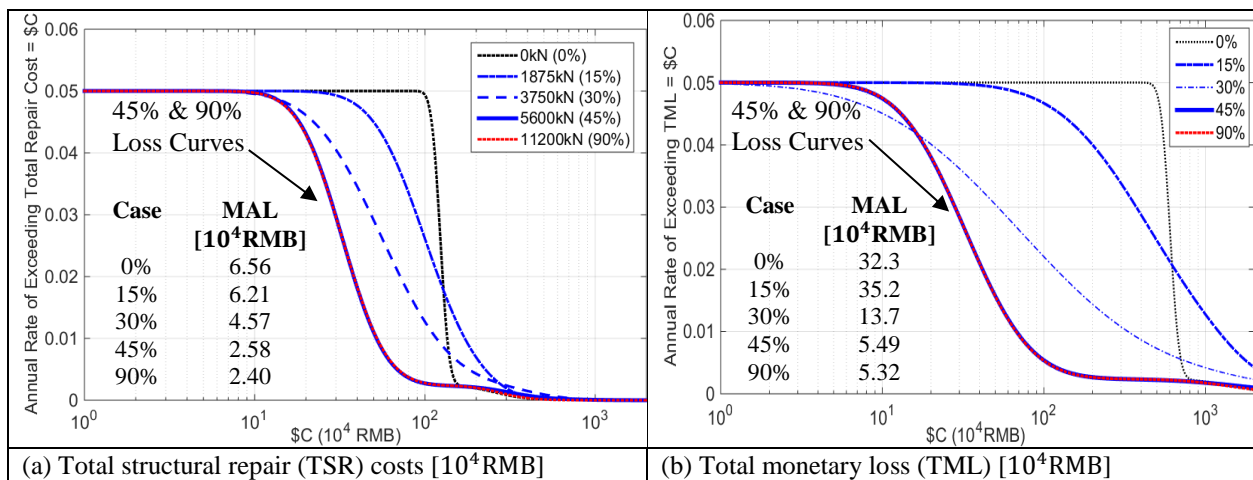


Figure 23 Loss curves and corresponding MAL values for each bridge model.

#### 4.4 Summary

A detailed seismic performance assessment of a typical four-span HSR MSSS bridge in the Sichuan-Yunnan Region has been systematically conducted in this chapter. The fragility curves were defined in order to quantitatively measure the seismic damage of each PG of the bridge model, and the fragility data obtained from testing data, design codes and engineering drawings.

The repair costs and related bridge closure time were also defined based on an investigation of the construction methodology of the HSR bridge and similar seismic retrofit projects due to 2008 Wenchuan earthquake in Sichuan province.

The results of the seismic performance show that the TTD costs constitute a major portion of the TMLs in all cases of the bridge model. Most of the TTD costs are attributed to PGs in the superstructure of the bridge, which can be relatively reduced using fixed bearings of low shear capacity under the MCE and DBE levels of ground motions. However, fixed bearings with low longitudinal restraint will rapidly increase both TTD and TSR costs under the SLE level of ground motions, which leads to a larger value of MAL. Hence, the cases with shear strength that are higher than 4900 kN has the lowest MAL. Further increasing the shear capacity of the fixed bearing will not effectively decrease MAL.

In conclusion, the bridge model of the 45%  $N_v$  case has the best overall seismic performance. However, this case will incur a huge financial loss that is at least 67.3 million RMB under MCE levels of ground motions. Moreover, the seismic performance of PGs related to EDPs of bridge bearings and girder joints cannot be effectively reduced by simply increasing the shear strength of the fixed bearings. Meanwhile, these PGs contributed a large portion of the TTD and TSR costs. Hence, it is recommended that seismic protective devices be incorporated in the HSR MSSS bridge system in order to further improve the seismic performance of the bridge system.

## **Chapter 5: Seismic Performance Evaluations and Optimizations of the HSR MSSS Bridge Using the Friction Pendulum System**

The purpose of this chapter is to develop a strategy to improve the seismic performance of the HSR MSSS bridge using seismic isolation devices. The advantages of using isolation devices will first be introduced and then compared. In addition, different optimal design methodologies for implementing isolation devices on bridges will be reviewed. This review shows that there is no consistent method for selecting the best design parameters for isolation devices. Hence, an innovative optimal method is proposed, one in which the optimal design of isolation devices is based on the PBEE framework. As well, the effectiveness of isolation devices is studied. Finally, the effects of the strict displacement-based design criteria for HSR bridges based on the optimal design will be investigated.

### **5.1 Literature Review of the FPS and its Optimal Design Methodologies**

Seismic isolation devices have been widely used for decades in bridges and buildings; the Friction Pendulum System (FPS) is one of the popular choices for the seismic retrofit of bridges, as seen with the Benicia-Martines Bridge (Zayas et al. 2001). In comparing FPS to other isolation devices, FPS is a cost-effective option with superior seismic performance and excellent durability. The restoring and frictional forces of the FPS do not vary with the frequency of ground motions (Jangid 2005), so the device can retain full functionality through its displacement range. Hence, the FPS not only displays great seismic responses under strong ground motions with multiple pulses or flings and long periods (Zayas et al. 1990), but also demonstrates a better performance

under weak ground motions (Tsopelas et al. 1996). Moreover, the FPS is good at minimizing adverse torsional motions (Jangid and Datta 1995) and restoring the excessive relative displacements developed between the sub- and superstructures of bridges. In addition, most FPSs are constructed from regular steel and are consequently significantly more economical than special materials such as shape memory alloys. They also exhibit improved durability as compared with conventional lead rubber bearings and viscous fluid dampers. Lastly, the FPS is easily incorporated into bridge retrofits by directly replacing the existing bearings, since FPSs can then be inserted into compact spaces and resist a wide range of vertical loading capacities.

However, innovative isolation devices have rarely been implemented in HSR bridge systems due to two major challenges: 1) A systematic seismic assessment of the HSR bridge system is required to quantify the direct and in-direct losses caused by different hazard levels of ground motions; and 2) A robust framework is required not only to optimize the design parameters of the FPS based on the system level of performance, but also to enable each key component of the HSR bridge to satisfy the strictly displacement-based design criteria.

The optimal design of seismic isolation devices has been extensively studied over the last decade. Early researchers mainly focused on using deterministic method to optimize the design parameters of the FPS based on a limited number of engineering performance objectives. For instance, Jangid (2005) optimized the isolation period and frictional coefficient ratio ( $\mu$ ) of the FPS based on deck acceleration and pier base shear, which the minimum seismic response of the isolated three-span continuous bridge can be achieved by using  $\mu$  in the range of 0.07 to 0.19. Furthermore, Lindt and Jiang (2014) optimized the isolation period of the FPS based on a regressive relationship derived from the results of nonlinear time-history analyses of six wood-frame structural models under 22 ground motions (van de Lindt and Jiang 2014). The performance

target of this optimization method only included spectral acceleration, and the  $\mu$  value of the FPS was assumed to be 0.07. The regression results and optimization equations from these deterministic methods cannot easily be implemented in other cases due to the variation in the performance targets and hazard levels of the ground motions.

With the rapid development of performance-based earthquake engineering, increasingly more researchers began to incorporate performance-based evaluation methods into the optimal design of the seismic retrofit of bridges ((Choi et al. 2004), (Padgett and DesRoches 2007), (Agrawal et al. 2012) and (Siqueira et al. 2014)). Zhang and Huo (Zhang and Huo 2009) optimized the characteristic strength and post yielding ratio of the FPS based on system fragility functions generated from the Probabilistic Seismic Demand Model (PSDM) with Incremental Dynamic Analysis (IDA). The uncertainties inherent in various levels of ground motions, structural material and geometry were considered in the investigation. However, the FPS was only optimized based on the damage probability of the bridge system, which has not considered the further impacts caused by the structural repair efforts and travel delay loss of the transportation system. Also, the system fragility function was calculated based on its component fragility functions with subjective weighted ratios, making it difficult to use in other types of bridge structures.

To overcome the above problems, the PBEE framework was employed for optimizing isolation devices based on decision variables of framework which include uncertainties inherent in each phase of the seismic assessments. Zhang's (Zhang and Shu 2014) and Xie's (Xie and Zhang 2016) optimization of the FPS have applied this framework to optimal design of FPS for buildings and bridges, in which the design parameters of the FPS are optimized based on the total loss ratio which is calculated based on the PBEE framework. The loss analysis in both



investigations only included the direct structural repair costs relative to the original construction costs, which is difficult to apply to large transportation networks like the HSR.

## 5.2 A Model Description of the FPS

The frictional sliding mechanism and re-centering capability are two key characteristics of single concave FPS. These characteristics can be demonstrated in a Free Body Diagram (FBD) of the FPS, as shown in Figure 24.

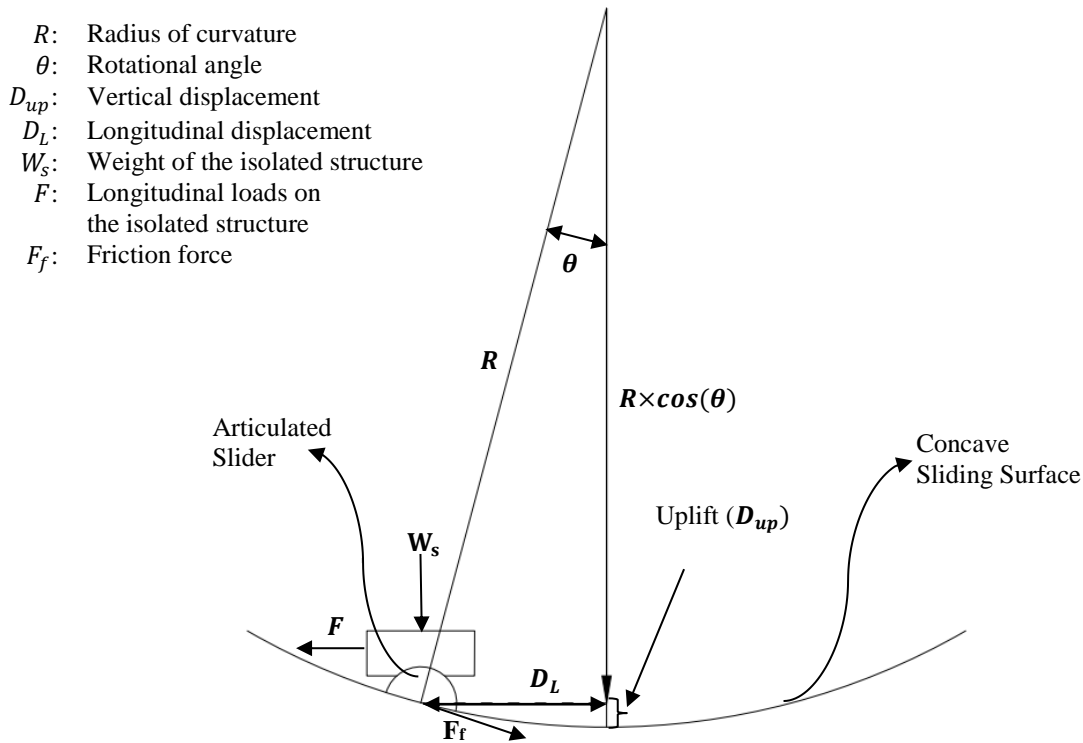


Figure 24 Free body diagram of a single concave FPS

Based on the FBD, the Force-Displacement (F-D) relationship of the FPS along the horizontal direction was derived as:

$$F = \frac{W_s}{R \cos \theta} D + \frac{F_f}{\cos \theta} \quad (2)$$

Since  $\theta$  is very small and  $\cos \theta$  is close to 1, Equation 2 can be re-written as:

$$F = \frac{W_s}{R}D + \mu W_s \text{sgn}(\dot{D}) \quad (3)$$

where  $W_s$  is the total weight supported on the FPS,  $R$  is the radius of curvature of the concave sliding surface,  $D$  is the lateral relative displacement between the superstructure and substructure,  $\mu$  is the friction coefficient and  $\text{sgn}(\dot{D})$  is a sign function. The first part of Equation 3 represents the restoration force provided by the single concave sliding surface, and the stiffness of this FPS is:

$$K_{FPS} = \frac{W_s}{R} \quad (4)$$

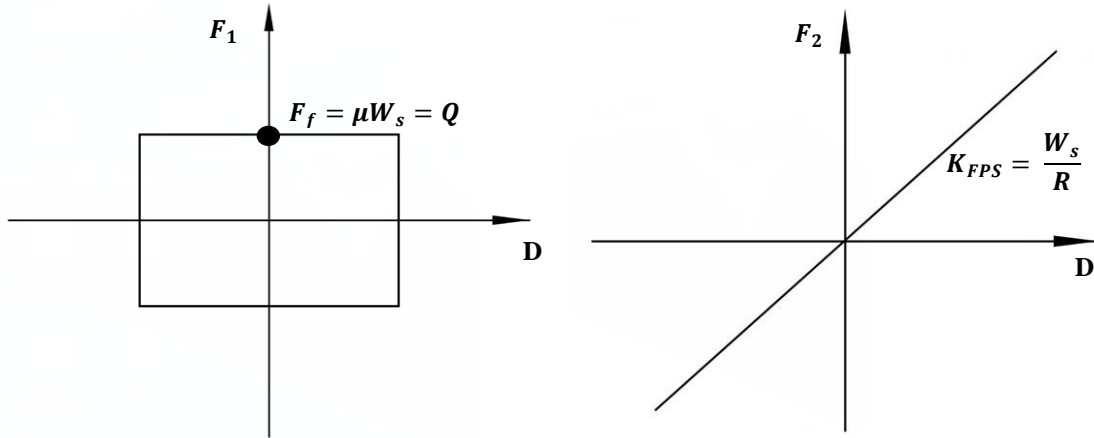
Based on Equation 3 and 4, the stiffness and the friction force are proportional to the total of the supported weight on the FPS, which enables the isolation device to effectively reduce the adverse torsional motions of the isolated structure. In addition, the natural period of vibration of the rigid isolated structure ( $T_{FPS}$ ) was derived as:

$$T_{FPS} = 2\pi \sqrt{\frac{m_s}{K_{FPS}}} = 2\pi \sqrt{\frac{R}{g}} \quad (5)$$

where  $g$  is the gravitational acceleration and  $m_s$  is the total mass supported on the FPS. Equation 5 demonstrates a unique property of FPS, the  $T_{FPS}$ , which is only related to the radii curvature of the FPS ( $R$ ) and it cannot be altered by the varying masses of isolated structures. On the other hand, this property enables designers to reduce the acceleration and inertial force of isolated structures by shifting their natural period of vibration at the expense of the increased relative displacement ( $D_L$ ).

In addition, the second part of Equation 3 represents the coulomb-friction damping shown in Figure 25 (a). This simple sliding mechanism retains the virtue of transmitting a limited inertia force of the rigid isolated structure which is as high as the maximum friction force ( $F_f$ ) from

superstructure to substructure under a wide range of frequency seismic loads. Meanwhile, the hysteretic frictional motion dissipates seismic energy and reduces the relative displacement ( $D$ ), which is the key threshold value for the seismic performance of HSR MSSS bridges. However, this comes at the price of increasing the seismic loads on the isolated structure since the effective stiffness of the system is increased by using a sliding material with a higher  $\mu$ .



(a) Coulomb friction model caused by a sliding mechanism at the interface

(b) Linear stiffness provided by the single concave pendulum of the FPS

**Figure 25 De-aggregation of hysteresis behaviors of FPS**

By combining the above two characteristics of the FPS, its hysteretic response can be represented by the bi-linear model shown in Figure 26. Then, the lateral resisting force of the FPS at a given time step,  $n$ , can be described as:

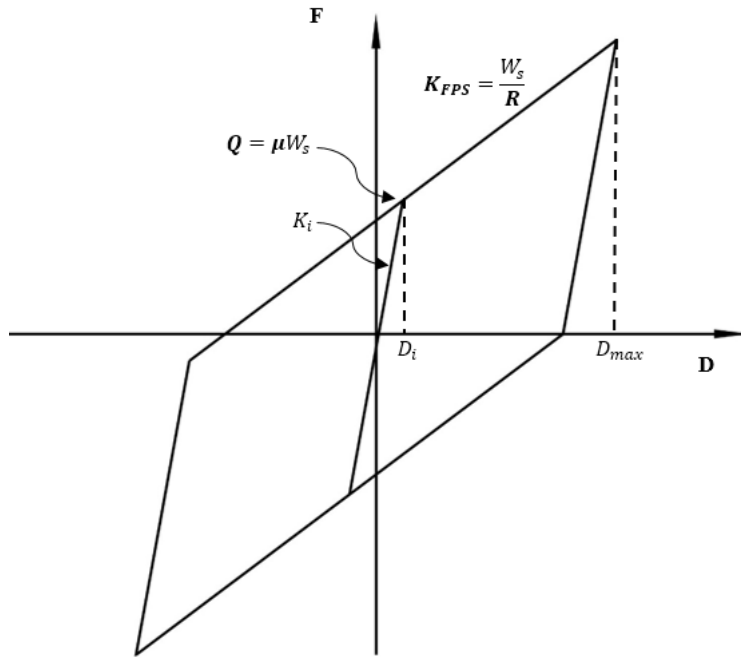
$$F(K_i, K_{FPS}, Q) = \begin{cases} \min(F_{n-1} + K_i(D_n - D_{n-1}), Q + K_{FPS}D_n), & \text{if } D_n > D_{n-1} \\ \max(F_{n-1} + K_i(D_n - D_{n-1}), -Q + K_{FPS}D_n), & \text{if } D_n < D_{n-1} \end{cases} \quad (6)$$

where  $K_i$  equals  $Q$  divided by  $D_i$ , and  $D_i$  is assumed to equal 2 mm, which identical to the assumption for the previous model of bridge bearings. The independent modelling parameters are  $K_{FPS}$  and  $Q$ , which are directly related to the  $R$  and  $\mu$  of the FPS. In addition, the  $R$  can be represented by  $T_{FPS}$  since the  $W_s$  in Equation 5 remains constant. Moreover, the dynamic property

of the original structural system is also an essential factor, so the  $T_{FPS}$  can be further described as a ratio of the fundamental vibration period of the structure with and without isolators:

$$TR = \frac{T_{FPS}}{T_{original}} \quad (7)$$

Consequently, isolation ratio ( $TR$ ) and friction coefficient ( $\mu$ ) of the sliding interface determine the optimal design of the FPS for minimizing TML based on the PBEE framework.



**Figure 26 Hysteresis model for the single concave FPS**

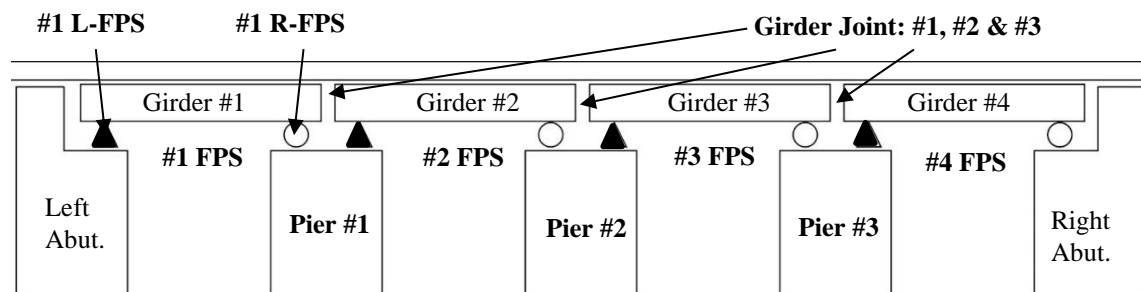
A wide combination of the design parameters ( $TR$  and  $\mu$ ) for the FPS are considered in this optimization study. The isolation period ratio ( $TR$ ) ranging from 0.5 to 3.5 with an increase of 0.25 and the friction coefficient ( $\mu$ ) ranging from 0.025 to 0.35 with an increase of 0.025 are included. This creates a total of 182 combinations. Table 13 shows the sum of the design parameters of the FPS included for this optimization study.

**Table 13 A Parametric study of the FPS with different sets of values for  $TR$  and  $\mu$**

$(TR_n, \mu_n)$	$\mu_1 (0.025)$	$\mu_2 (0.050)$	...	$\mu_{14} (0.350)$
$TR_1 (0.50)$	(0.50, 0.025)	(0.50, 0.050)	...	(0.50, 0.350)
$TR_2 (0.75)$	(0.75, 0.025)	(0.75, 0.050)	...	(0.75, 0.350)
...	...	...	...	...
$TR_{13} (3.50)$	(3.50, 0.025)	(3.50, 0.050)	...	(3.50, 0.350)

### 5.3 A Model Description of the Isolated four-span HSR MSSS bridge

The FPS was incorporated into the typical four-span HSR MSSS bridge model by replacing the original bearings, shown in Figure 27. The material model of all the bearing elements shown in Figure 8 was changed from the EPP to the bilinear material model shown in Figure 26. In addition, the FPS on the left end of each girder (L-FPS) is assumed to be equipped with shear rods. Hence, L-FPSs can behave like normally fixed bearings, providing fixity and transferring design loads from the super- to substructure. Moreover, 5625 kN (45%  $N_v$ ) was selected as the shear capacity for the shear rods of L-FPSs.



**Figure 27 Schematic diagram of an isolated four-span HSR MSSS bridge**

The damage and loss analyses of PGs that have EDPs related to bearing displacement were modified. The peak longitudinal relative displacement between the articulated slider and its supporting sliding surface is defined as the EDP for measuring the seismic performance of the FPS PG and the track-slab PG. Following this, two damage states were defined for FPS PGs. These

DSs are: 1) no damage and 2) FPS unseating failure. The EDP limit of DS2 was defined as 600 mm, which is the maximum allowable sliding width between the center of the original bridge bearing and the edge of its concrete pedestal. It should be noted that the re-centering capability of the single concave FPS largely reduces the repair efforts for restoration of girder positions. Thus, the damage states of this PG are reduced from three to two. In addition, the repair actions and associated costs for the FPS unseating failure remain the same as before; this analysis is summarized in Table 14.

**Table 14 Loss analysis of FPS**

Repair Items	Units	FPS			Unit Cost [¥10 <sup>4</sup> RMB]		
		DS1	DS2	Max. cost	Min. Cost	Max. Qty.	Min. Qty.
<b>FPS replacement</b>	# of FPS	0	2	4.5	1.5	2000	1
<b>Jacking up of girder</b>	-	0	2	15.35	15.35	1000	1
<b>Long. position restoration (girder)</b>	-	0	2	5	5	1000	1
<b>Downtime</b>	# of Days	0	1	240	240	1000	1

As well, the DSs of the track-slab PG were reduced from four to three, as shown in Table 15. The repair actions and costs for the corresponding damage states are the same as those of the previous assessment shown in chapter 4.

**Table 15 Damage analysis of track PG with FPS**

	>DS2	>DS3
EDP [mm]	600 mm	1450mm
Damage Mechanism	Girder falls out of the concrete pedestal	Girder falls out of the pier

Based on the modified fragility data, new fragility curves were generated and shown in Figure 28. Following this, the seismic performance assessment could be performed for the isolated HSR MSSS bridge system, with 182 cases of FPSs based on the procedures shown in chapter 4.

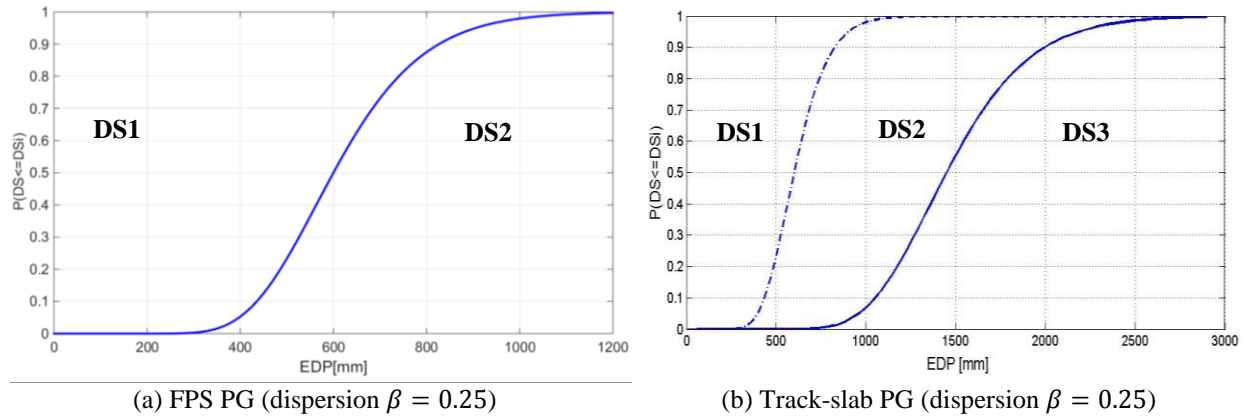


Figure 28 Modified fragility curves for related PG of the isolated four-span HSR MSSS bridge

#### 5.4 Allowable Ranges of Design Parameters of the FPS

As discussed in Chapter 5.2, FPS has only two control parameters ( $TR$  and  $\mu$ ). However, not all parameters can be used for the HSR MSSS bridge system. Three causes need to be considered: 1) When the relative displacement of the FPS ( $D_L$ ) is too large, it will lead to an adverse uplift of the bridge girder; 2) When the compressive displacement of the girder joint is too large, it will cause pounding damage in the bridge girders and compressive cracks in the roadbed; and 3) When  $\mu$  is excessively high, it will result in significant structural damage to the bridge pier. The following sections, 5.4.1 to 5.4.3, will address these considerations sequentially.

##### 5.4.1 The Boundary Conditions Imposed by the FPS

An uplift ( $D_{up}$ ) of the isolated superstructure of the bridge will be caused by the  $D_L$  of the FPS PGs. Excessive uplift of the bridge girders will easily damage the roadbed and track-slab systems, so the maximum allowable uplifting distance ( $D_{upm}$ ) of the superstructure is 5 mm. for the past retrofits of the HSR MSSS bridge bearings (Yu 2015 and Song et al. 2014). In order to compare the seismic responses of each FPS with a 5 mm.  $D_{up}$ , the  $D_{up}$  limit needs to be

transferred to the  $D_L$  limits for each pair of  $TR$  and  $\mu$  values. Based on Equation 8, the  $D_{L_m}$  can be calculated for each  $TR$  value (Appendix A), for which the calculated results are listed in Table 16. In addition, the  $D_{L_m}$  is independent of  $\mu$ , so a 3-D boundary surface can be generated and compared with the seismic response for each FPS.

$$D_{L_m} = \sqrt{0.010 \left( \left( \frac{TR \times T_1}{2\pi} \right)^2 \times g \right) - (D_{up_m})^2} \quad (8)$$

**Table 16** The calculated  $D_{L_m}$  [mm] for each of the  $TR$

<b><math>TR</math></b>	0.5	0.75	1	1.25	1.5	1.75	2	2.25	2.5	2.75	3	3.25	3.5
<b><math>D_{L_m}</math></b>	12	26	39	52	65	78	91	104	117	130	143	156	169

Figure 29 shows that the EDP ( $D_L$ ) of all the R-FPS were plotted as a function of  $TR$  and  $\mu$ . Comparing the values presented in Table 16 with the EDPs plotted in Figure 29 shows that the allowable design parameters are summarized as the shaded area shown in Figure 30. Hence, the allowable ranges of the design parameters of the FPS are  $\mu > 0.15$  and  $TR > 2$ .



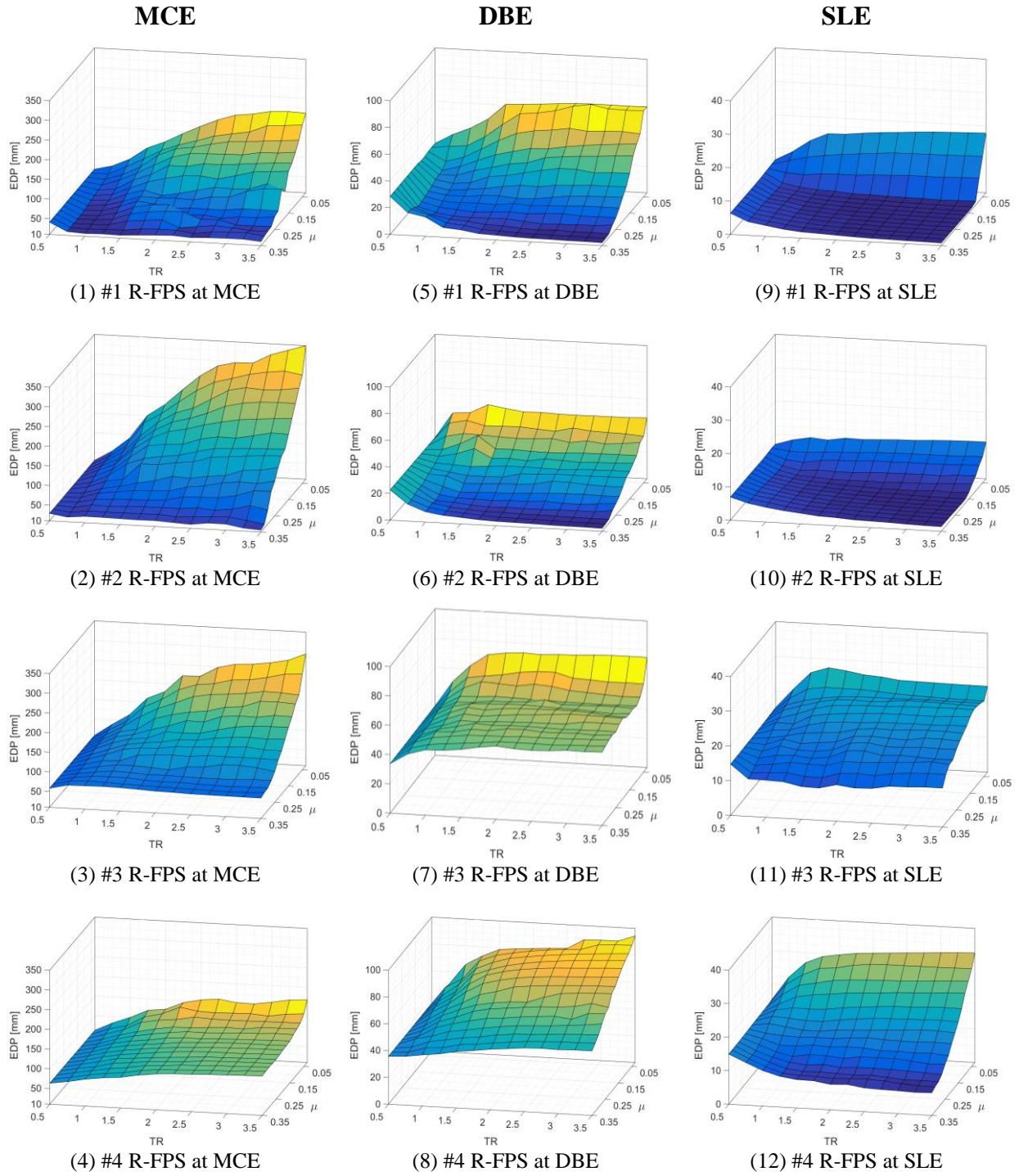
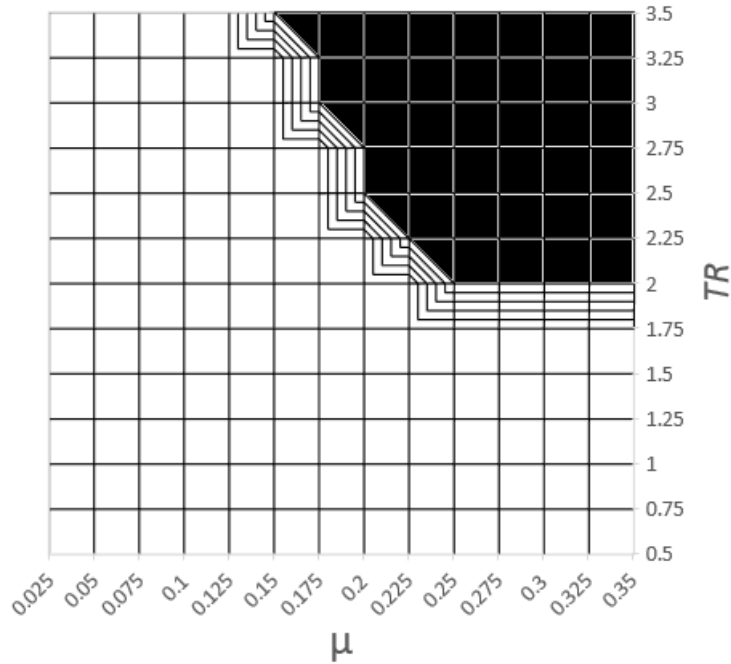


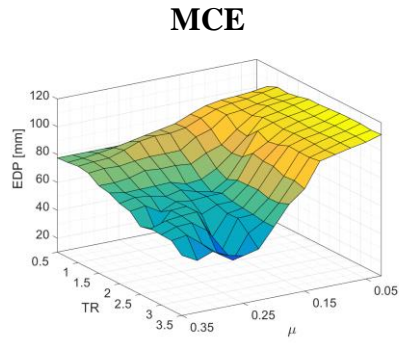
Figure 29 The plots of median longitudinal peak displacement of R-FPS vs.  $TR$  and  $\mu$



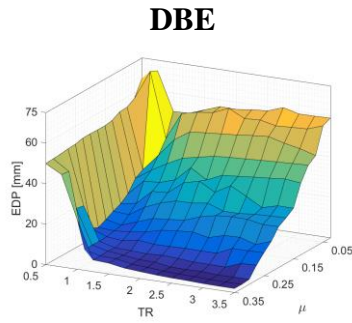
**Figure 30** The boundary condition of  $TR$  and  $\mu$  imposed by the uplift of the FPS

#### 5.4.2 The Boundary Condition Imposed by Girder Joints

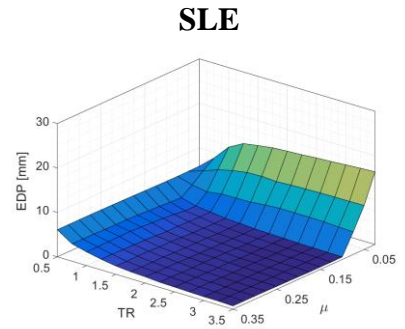
Figure 31 shows the EDPs (median peak compressive displacements) of the three girder joints illustrated in Figure 27 under the three proposed hazard levels. The EDP limit of the girder joints is assumed to be 65 mm., avoiding the collisions between the girders and the compressive strength degradation of the roadbed. A comparison of the EDPs plotted in Figure 31 with the EDP limit reveals the allowable design parameters, as summarized in Figure 32. As a result, the current allowable ranges of the design parameters of FPS are:  $\mu > 0.275$  and  $TR > 2$ .



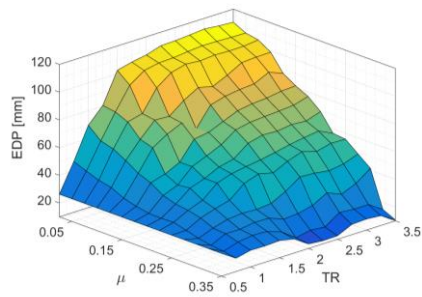
(1) #1 Girder joint at MCE



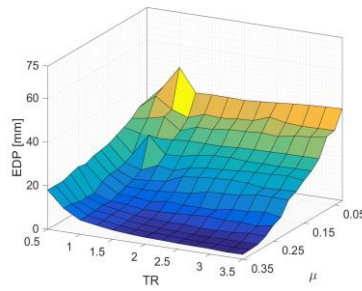
(4) #1 Girder joint at DBE



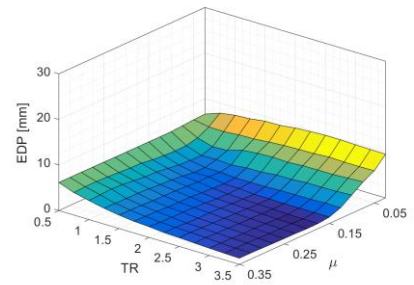
(7) #1 Girder joint at SLE



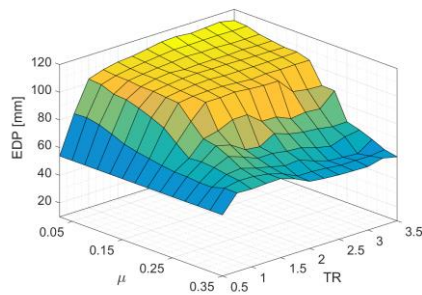
(2) #2 Girder joint at MCE



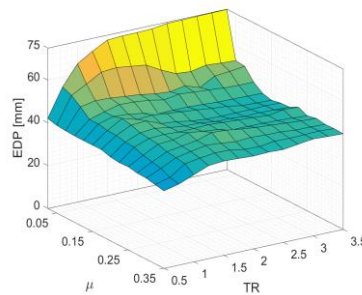
(5) #2 Girder joint at DBE



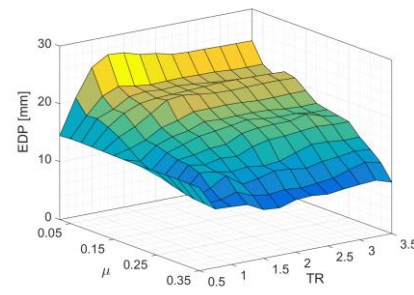
(8) #2 Girder joint at SLE



(3) #3 Girder joint at MCE



(6) #3 Girder joint at DBE



(9) #3 Girder joint at SLE

**Figure 31 3-D plots of the median peak displacements of the girder joints (compressional) vs.  $TR$  and  $\mu$**

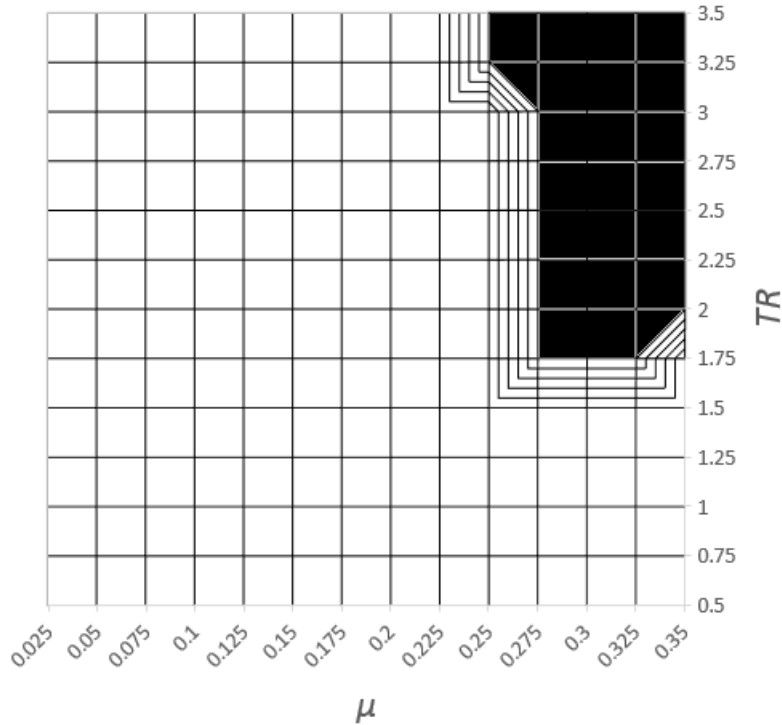


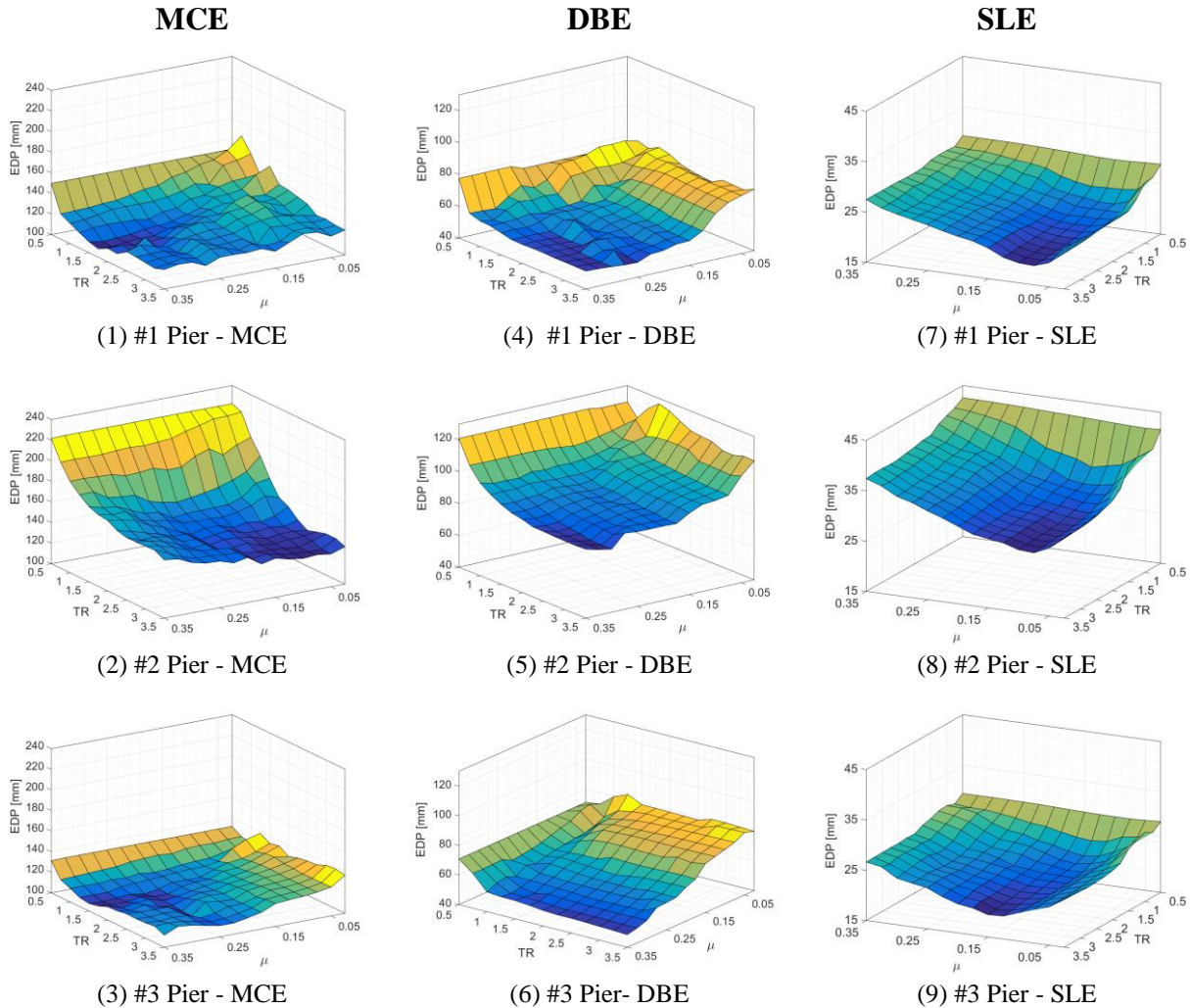
Figure 32 The boundary conditions of  $TR$  and  $\mu$  imposed by the EDP limit of the girder joints

### 5.4.3 The Boundary Condition Imposed by the Piers

Figure 33 shows the EDPs (pier-top drift) of the three piers illustrated in Figure 27 under the three proposed hazard levels. The bridge system using an FPS with a high value of  $\mu$  will transfer larger seismic loads from the superstructure to the foundation through the piers. To prevent the pier PGs from experiencing severe cracking and degradation, it has been proposed that the pier-top drift (EDP) of the pier PGs be smaller than 320 mm.

Based on the EDPs shown in Figure 33(1), (2) and (3), the peak EDPs with  $TR > 2$  and  $\mu > 0.275$  are: #1 Pier) 118mm, #2 Pier) 156 mm and #3 Pier) 114 mm. None of these values exceed the 50% of the EDP limit of the DS3 (320 mm) of the 16-m pier PGs. Hence, the damages

in the isolated bridge piers will be limited to moderate cracks that will not cause any bridge closures or traffic delays of the HSR lines.



**Figure 33** The 3-D plots of the longitudinal median peak pier-top displacement vs.  $TR$  and  $\mu$

### 5.5 The Optimized Ranges of the Design Parameters of FPS

The PBEE framework can be used to facilitate creation of an optimal design for the FPS by quantitatively transferring all the types of seismic responses of the structure system into a universal decision variable (TML). Then, the total monetary losses of the bridge model under several hazard levels can be represented as one performance index, MAL. Hence, the design

parameters ( $TR$  and  $\mu$ ) of the FPS can be directly optimized based on finding the design scenarios by which the isolated bridge produced the lowest values of MAL under selected hazard levels of ground motion.

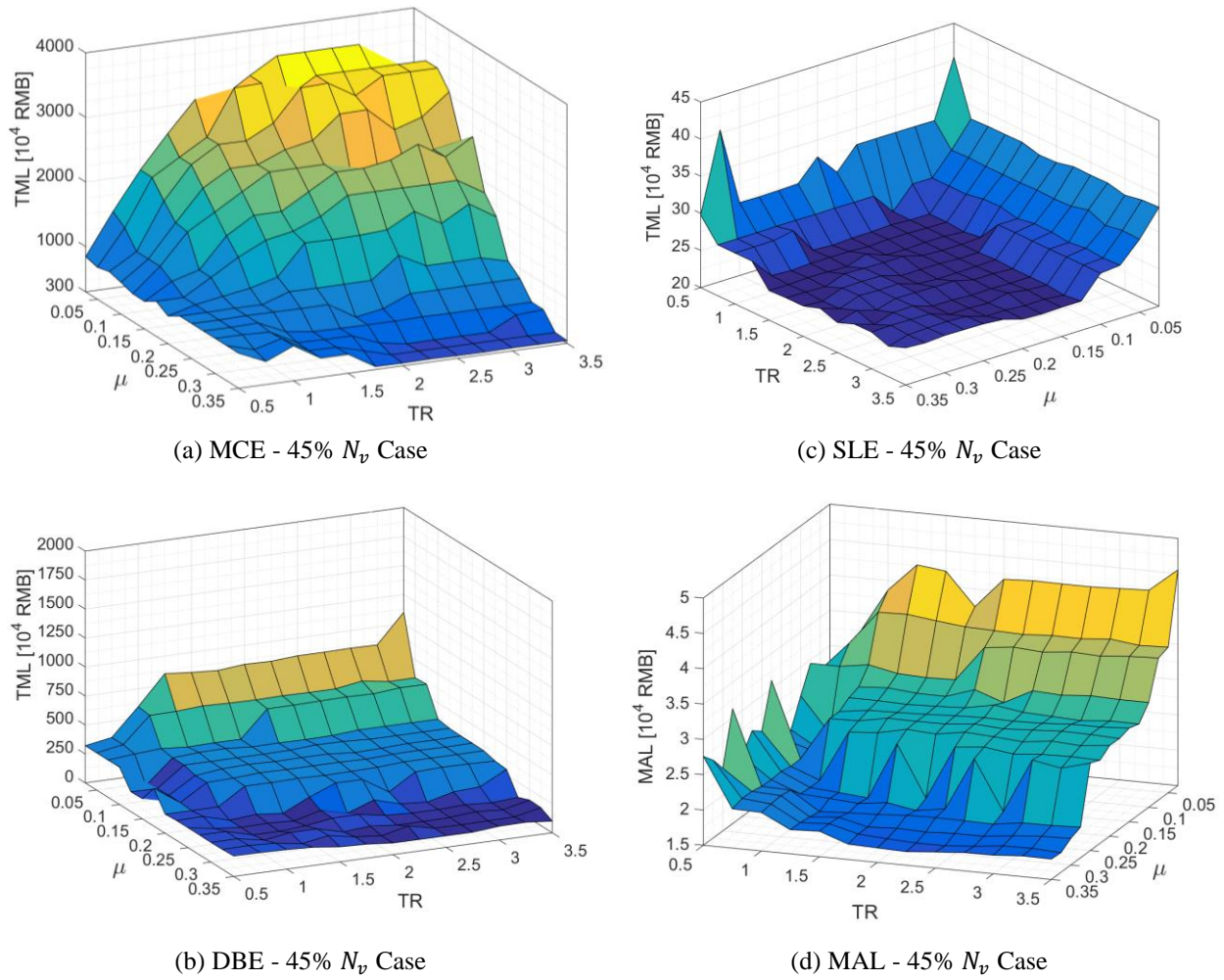
The seismic performances of the isolated bridge model with its 182 cases of FPS under three hazard levels have been evaluated. The TMLs and MALs of all cases of the bridge model were plotted as functions of  $TR$  and  $\mu$ , as shown in Figure 34. For the 45%  $N_v$  case at the MCE level shown in Figure 34 (a), the  $TR$  has negligible impact on the TML when the value of  $TR$  is greater than 2. However, the TML decreases as the  $\mu$  is increases. A similar trend can be observed in Figure 34 (b) and (c).

For further facilitating decision makers to select the best combination of design parameters for the FPS, the MAL was calculated and displayed in Figure 34(d). It demonstrates that the lowest level of MAL can be attained when  $\mu$  ranges from 0.275 to 0.35, while  $TR$  is larger than 2. It should be noted that these optimum ranges of the design parameters of FPS differ from the optimized FPSs for isolated building structures. The priority of the optimized FPSs of the HSR MSSS bridge system is to systematically control the displacement developed in each component of the HSR bridge superstructure.

The effectiveness of using FPSs with optimum design parameters is demonstrated in Table 17. The median TML of the isolated bridge (the 45%  $N_v$  case) at all three hazard levels is reduced by greater than 90% when compared to the most optimized TML (TSR+TTD) of the non-isolated four-span HSR MSSS bridge shown in Table 12. It should be noted that the median TML of the isolated bridge model is calculated based on the values of TML within the optimum ranges of the design parameters ( $\mu > 0.275$  and  $TR > 2.0$ ). Table 17 also shows that the optimized MAL value is reduced to 31% relative to the MAL value of the previous non-isolated bridge model.



**Isolated HSR MSSS bridge (45%  $N_v$  Case)**



**Figure 34 TML vs.  $TR$  and  $\mu$  of FPSs under MCE, DBE and SLE levels of ground motions.**

**Table 17 A comparison of seismic performances of the prototype HSR MSSS bridge with and without FPS**

	<b>TML at MCE</b>	<b>TML at DBE</b>	<b>TML at SLE</b>	<b>MAL</b>
45% $N_v$ bridge without isolation (Million RMB)	67.09	16.66	2.66	$2.58 \times 10^{-2}$
45% $N_v$ bridge with optimum FPS (Million RMB)	3.54	1.03	0.25	$1.78 \times 10^{-2}$
Percentage of reduction (%)	<b>95%</b>	<b>94%</b>	<b>91%</b>	<b>31%</b>

## 5.6 Summary

Based on this optimization methodology, the balanced seismic responses of the 45%  $N_v$  case isolated bridge model are attained using the FPS with  $TR > 2$  and  $\mu > 0.275$ . The longitudinal relative displacements developed at FPSs and girder joints are minimized, and the pier-top drift is limited to less than 160 mm. In addition, the peak uplifts of FPSs are restricted to below 5 mm.

As a result, the seismic performance of the four-span HSR MSSS bridge is significantly improved by using FPS optimization based on the PBEE framework. The TML of the isolated bridge has been reduced more than 90 percent under each hazard level. The 3-D plot of MAL and the 2-D plot of the boundary conditions have been developed not only for selecting the best combination of design parameters for the FPS, but also for enabling the seismic response of the isolated HSR bridge, satisfying all the strict requirements imposed by the functionality of the HSR lines.



## Chapter 6: Summary and Conclusion

### 6.1 Summary and Conclusion

The structural characteristics of the HSR MSSS bridge system are very different from those of conventional highway MSSS bridges. The current seismic assessment methodologies used for highway MSSS bridges cannot be applied directly to the HSR MSSS bridge system. Hence, this study has systematically developed a seismic loss assessment framework to thoroughly assess the seismic performance of the HSR MSSS bridge system in Southwest China.

Key structural and non-structural components such as the CRTS II track-slab system are included. The nonlinearities of key structural components, such as piers and bearings, have been calibrated based on experimental data, and advanced simulation techniques such as direct element removal have been implemented. A detailed nonlinear dynamic analysis of a typical four-span bridge model with fixed bearings at five levels of shear strength was investigated in this study. The results show that the seismic performance of the HSR MSSS bridge system is highly dependent on the damage states of the bearings. Several major findings are listed below:

1. TTD costs constitute the major portion of the TML
2. Most of the TTD costs are attained from the CRTS II track-slab performance group.
3. A detailed parameter study was conducted, with the result revealing that the seismic performance of the CRTS II track-slab system cannot be effectively controlled using the shear strength of the bearings.

4. The HSR MSSS bridge with fixed bearings at 45%  $N_v$  has the best overall seismic performance; however, despite this finding, the HSR MSSS bridge continues to precipitate a loss of 67.3 million RMB at the MCE level.
5. The HSR MSSS bridge with fixed bearings at 15%  $N_v$  has the worst overall seismic performance under the SLE hazard levels.
6. The MAL is largely acquired at the SLE hazard level, due to the high rate of return.

To improve the seismic performance of the HSR MSSS bridge, a seismic protective device, being a single-concaved FPS, has been incorporated into this HSR MSSS bridge system. The PBEE framework with its previously developed hazard, damage and loss analyses was utilized for the optimal design of the FPS. Based on the proposed optimization methodology, several major findings are summarized as below:

1. The PBEE framework can be used as an effective tool to optimize the design of the FPS and ensure a safe distribution of seismic damages for the bridge piers, FPS and superstructure components.
2. Based on the optimization presented in this study, the optimal parameters of FPS are  $TR > 2$  and  $\mu > 0.275$ . The TML of the isolated bridge model decreased more than 90% under all considered levels of ground motions.

## 6.2 Future Research

In order to further understanding of the seismic performance of the HSR bridge systems, additional experimental studies and further numerical analyses were recommended, which are summarized below:

1. The failure mechanism of the non-ballasted track-slab systems under strong ground motion requires further experimental investigation. The nonlinear behavior and corresponding damage states of the components of the non-ballasted track-slab system under strong cyclic loads likewise necessitate further study.
2. It is recommended that a database be constructed for further data collection concerning repair costs and effort, and travel delay loss from similar retrofit projects nationwide. This would be a fundamental step in further implementing the PBEE framework into the entire HSR line.
3. The plastic hinge is easily developed in the fixed bearings, which require further validation based on experimental investigation. It is recommended that the fixed bearings and their connected parts, such as concrete pedestals, the upper regions of the piers and lowermost precincts of the girders, be included in experimental investigations.
4. The interactions between the high-speed trains and the HSR MSSS bridge under strong earthquake loads are recommended to be considered for the further optimal design of seismic protective devices.

## Bibliography

- Agrawal, a. K., Ghosn, M., Alampalli, S., and Pan, Y. (2012). “Seismic Fragility of Retrofitted Multispan Continuous Steel Bridges in New York.” *Journal of Bridge Engineering*, 17(4), 562–575.
- Ancheta, T. D., Darragh, R. B., Stewart, J. P., Seyhan, E., Silva, W. J., Chiou, B. S.-J., Wooddell, K. E., Graves, R. W., Kottke, A. R., Boore, D. M., Kishida, T., and Donahue, J. L. (2014). “NGA-West2 Database.” *Earthquake Spectra*, Earthquake Engineering Research Institute , 30(3), 989–1005.
- Aparicio, A. (2008). “Differences in designing high-speed railway bridges and highway bridges.” *Bridges for High-Speed Railways: Revised Papers*.
- ASCE. (2010). *Minimum design loads for buildings and other structures. ASCE standard*.
- CEA. (2015). *Seismic ground moition parameteres zonation map of China (GB 18306-2015)*. China Standards Publishing House.
- CEN. (2005). *EN 1993-1-8:2005 - Eurocode 3: Design of steel structures - Part 1-8: Design of joints. Eurocode 3*.
- China CR. (2006). *Code for seismic design of railway engineering (GB50111-2006) [in Chinese]*. China Railway Ministry.
- China MOHURD. (2010). *Code for design of concrete structures (GB50010-2010) [in Chinses]*. Ministry of Housing and Urban-Rural Development.
- Choi, E., DesRoches, R., and Nielson, B. (2004). “Seismic fragility of typical bridges in moderate seismic zones.” *Engineering Structures*, 26(2), 187–199.
- CRC. (2012). *Code for Design of Railway Continuous Welded Rail (TB 10015-2012)*. China

- Railway Publishing House.
- CRC. (2013). “Spherical bearings for railway bridges (TB/T 3320-2013).” China Railway Publishing House.
- FEMA, P. (2012). “58-1 Seismic Performance Assessment of Buildings.” *Federal Emergency Management Agency*.
- Hoshikuma, J., Kawashima, K., Nagaya, K., and Taylor, A. W. (1997). “Stress-Strain Model for Confined Reinforced Concrete in Bridge Piers.” *Journal of Structural Engineering*, 123(5), 624–633.
- Hu, S., Niu, B., Ke, Z., and Liu, X. (2013). “Study on the Optimization of Standard Span Length Simply Supported Box Girder for High-Speed Railway.” *China Railway Science*, 34(1), 15–21.
- Jangid, R. S. (2005). “Optimum friction pendulum system for near-fault motions.” *Engineering Structures*, 27(3), 349–359.
- Jangid, R. S., and Datta, T. K. (1995). “Performance of Base-Isolation Systems for Asymmetric Building Subject To Random-Excitation.” *Engineering Structures*, 17(6), 443–454.
- Jiang, L., Shao, G., Jiang, J., and Wang, H. (2013). “Experimental study on seismic performance of solid piers with round ended cross-section in high-speed railway.” *China Civil Engineering Journal*, 46(3), 86–95.
- Jiang, X. (2015). “Analysis of the Indices of the Engineering Cost of Ballastless Tracks.” 5–9.
- Ketchum, M. (2004). “Influence of design ground motion level on highway bridge costs.” *PEER Lifelines Project*.
- Kim, S. H., Mha, H. S., and Lee, S. W. (2006). “Effects of bearing damage upon seismic behaviors of a multi-span girder bridge.” *Engineering Structures*, 28(7), 1071–1080.

- Li, Y. (2014). "PERFORMANCE-BASED DESIGN AND EVALUATION OF INNOVATIVE STEEL KNEE BRACED TRUSS MOMENT FRAMES." University of British Columbia.
- van de Lindt, J. W. and, and Jiang, Y. (2014). "Empirical Selection Equation for Friction Pendulum Seismic Isolation Bearings Applied to Multistory Woodframe Buildings." *Practice Periodical on Structural Design and Construction*, 19(3), 1–10.
- Liu, X. (2015). "Analysis of CRTS III Type Plate Ballastless Track Structure and Cost." *Railway Engineering Cost Management*, (3), 5–9.
- Mackie, K. R., Wong, J.-M., and Stojadinovic, B. (2008). "Integrated Probabilistic Performance-Based Evaluation of Benchmark Reinforced Concrete Bridges." *Peer*, (January), 199.
- Mackie B., K. and S. (2003). "Seismic demands for performance based design of bridges." *PEER Report 2003/16*, (August).
- Mander, J. B., Priestley, M. J. N., and Park, R. (1988). "Observed Stress-Strain Behavior of Confined Concrete." *Journal of Structural Engineering*, 114(8), 1827–1849.
- P. Mander, J. B. ;Priestley. M. J. N. . P., Priestley, M. J. N., and Park, P. (1989). "Theoretical Stress-Srain Model for Confined Concrete." *Journal of Structural Engineering*, 114(8), 1804–1826.
- Padgett, J. E., and DesRoches, R. (2007). "Bridge functionality relationships for improved seismic risk assesment of transportation networks." *Earthquake Spectra*, 23(1), 115–130.
- PEER. (2017). "Open system for earthquake engineering simulation (OpenSees) framework - version 2.5.0." Pacific Earthquake Engineering Research Center, Univ. of California, Berkeley.
- Ran, Q. (2009). "Restoration of Bridge Girder Position for G213 Highway Bridges Between Wenchuan - Yinxiu." *Southwest Highway*, 2, 35–37.

- SCED. (2017). “Daily Ridership of Cheng-Mian-Le Inter-City High-speed Railway Increased 107.8 percentage.” *SCED*, <<http://www.sced.cn/html/xwpd/tour/87139.html>>.
- Scott, B. D., Park, R., and Priestley, M. J. N. (1982). “Stress-Strain Behavior of Concrete Confined by Overlapping Hoops at Low and High Strain Rates.” *Journal Proceedings*, 79(1), 13–27.
- Sezen, H., and Moehle, J. P. (2004). “Shear strength model for lightly reinforced concrete columns.” *Journal of Structural Engineering*, 130(11), 1692–1703.
- Shao, G., Jiang, L., and Chouw, N. (2014). “Experimental investigations of the seismic performance of bridge piers with rounded rectangular cross-sections.” *Earthquake and Structures*, 7(4), 463–484.
- Shen, D., Ji, B., Sun, Q., Tang, X., Zheng, H., and Rui, F. (2012). “Analysis and Estimation on Cost of Bridge Synchronous Jacking up Project.” *Construction Economy*, 5, 32–34.
- Siqueira, G. H., Sanda, A. S., Paultre, P., and Padgett, J. E. (2014). “Fragility curves for isolated bridges in eastern Canada using experimental results.” *Engineering Structures*, Elsevier Ltd, 74, 311–324.
- Smith, K. (2017). “China Railway sets out 2017 targets.” *International Railway Journal*, <<http://www.railjournal.com/index.php/financial/china-railway-sets-out-2017-targets.html>> (Mar. 1, 2017).
- Song, F., Shi, Q., Ban, X., and Dong, J. (2014). “The Study of Replacing Pot-rubber Bearing for Simply Supported Box Girder Bridge of High-Speed Railway.” *Railway Engineering*, (July), 4–7.
- Sun, S. (2008). “Bridge engineering in Beijing–Shanghai high-speed railway.” *Railway Standard Design*, 6, 1–4.
- Talaat, M., and Mosalam, K. M. (2009). “Modeling progressive collapse in reinforced concrete

- buildings using direct element removal.” *Earthquake Engineering & Structural Dynamics*, John Wiley & Sons, Ltd., 38(5), 609–634.
- Terzic, V., Stojadinović, B., and Department of Civil and Environmental Engineering Berkeley, U. of C. (2010). “Post-Earthquake Traffic Capacity of Modern Bridges in California.” 3(2010/ 103), 218.
- The Economist. (2017). “China has built the world’s largest bullet-train network.” *The Economist*, <<http://www.economist.com/news/china/21714383-and-theres-lot-more-come-it-waste-money-china-has-built-worlds-largest>> (Mar. 2, 2017).
- Tsopelas, P., Constantinou, M. C., Kim, Y. S., and Okamoto, S. (1996). “Experimental Study of FPS System in Bridge Seismic Isolation.” *Earthquake Engineering and Structural Dynamics*, 25(4), 65–78.
- Waugh, J. (2009). “Nonlinear analysis of T-shaped concrete walls subjected to multi-directional displacements.” *Ph.D. Dissertation*, Iowa State University.
- Wu, J., Wang, C., He, X., Wang, X., and Li, N. (2017). “Spatiotemporal changes in both asset value and GDP associated with seismic exposure in China in the context of rapid economic growth from 1990 to 2010.” *Environmental Research Letters*, 12.
- Xie, Y., and Zhang, J. (2016). “Optimal Design of Seismic Protective Devices for Highway Bridges Using Performance-Based Methodology and Multiobjective Genetic Optimization.” *Journal of Bridge Engineering*, 22(2009), 4016129.
- Xu, S. (2010). “Bridge Design of Beijing - Shanghai HSR line.” *Railway*, 2010(7), 41–45.
- Yan, B., Dai, G.-L., and Hu, N. (2015). “Recent development of design and construction of medium and long span high-speed railway bridges in China.” *Engineering Structures*, Elsevier Ltd, 100, 707–717.



- Yang, T. Y., Moehle, J., Stojadinovic, B., and Kiureghian, A. Der. (2009). “Seismic Performance Evaluation of Facilities :” *Journal of Structural Engineering*, 135(10), 1146–1154.
- Yong, C., and Booth, D. C. (2011). *The Wenchuan Earthquake of 2008: Anatomy of a Disaster*. Springer Science & Business Media.
- Yu, Z. (2015). “The Methodology of Adjusting the Position of High-speed Railway Bridge Bearings.” *Railway Engineering*, (September), 32–34.
- Zayas, V. A., Eeri, M., Low, S. S., Mahin, S. A., and Eeri, M. (1990). “A Simple Pendulum Technique for Acheiving Seismic Isolation.” *Earthquake Spectra*, 6(2), 317–333.
- Zayas, V. A., Low, S., Mokha, A. S., and Imbsen, R. A. (2001). “Seismic Isolation of Benicia-Martinez Bridge.” *Structures Congress 2014*, 3–8.
- Zhang, J., and Huo, Y. (2009). “Evaluating effectiveness and optimum design of isolation devices for highway bridges using the fragility function method.” *Engineering Structures*, Elsevier Ltd, 31(8), 1648–1660.
- Zhang, J., and Shu, Z. (2014). “Optimal Design of Isolation Devices for Buildings Using Performance Based Methodology.” (310), 1–34.
- Zhu, Q. (2013). “Interaction between simply supported beams and CRTS II slab ballastless track.” Central South University.

## Appendices

### Appendix A : Additional Design Parameters for the FPS

The radius curvature and uplift of the FPS were calculated in this section.

#### A.1 The Radius Curvature of the FPS

Based on the Equation 5 in Section 5.2, the radius curvature ( $R$ ) of the FPS can be calculated as Equation (1). In addition, the fundamental period of the isolated structure is represented as a ratio of the period of the original structure, which is  $T_{FPS} = TR \times T_1$ . Hence,  $R$  can be written as Equation (2). Then,  $R$  is calculated based on  $T_1 = 1.0435$  sec., with  $TR$  ranging from 0.25 to 3.5, as shown in Table 18. It should be noted that  $R$  is positively correlated with the  $TR$  of the FPS.

$$R = \left( \frac{T_{FPS}}{2\pi} \right)^2 \times g \quad (1)$$

$$R = \left( \frac{TR \times T_1}{2\pi} \right)^2 \times g \quad (2)$$

**Table 18 The radius of curvature of the FPS w.r.t to each TR ratio**

$TR$	0.50	0.75	1.00	1.25	1.50	1.75	2.00	2.25	2.50	2.75	3.00	3.25	3.50
$R$ [m]	0.068	0.152	0.271	0.423	0.609	0.829	1.082	1.370	1.691	2.046	2.435	2.858	3.315

#### A.2 Uplift of the FPS

Based on the free body diagram of the FPS shown in Figure 24, the uplift due to the longitudinal displacement ( $D_L$ ) of the articulated slider can be calculated as Equation (3). Based on the assumption that  $D_L = 100$  mm, the corresponding  $D_{up}$  was calculated and listed in Table 19.

$$D_{up} = R - \sqrt{R^2 - D_L^2} \quad (3)$$

**Table 19 Uplift w.r.t to each TR ratio**

<b>TR</b>	0.50	0.75	1.00	1.25	1.50	1.75	<b>2.00</b>	2.25	2.50	2.75	3.00	3.25	3.50
<b>R [m]</b>	0.068	0.152	0.271	0.423	0.609	0.829	<b>1.082</b>	1.370	1.691	2.046	2.435	2.858	3.315
<b><math>D_{up}</math> [mm]</b>	-	37.46	19.16	12.00	8.27	6.06	<b>4.63</b>	3.66	2.96	2.44	2.05	1.75	1.51

### A.3 The Maximum Allowable Longitudinal Displacement of FPS

Based on the F.B.D presented in Figure 24, the relationship between  $D_{upm}$  and  $D_{Lm}$  is shown in Equation (4), with  $D_{upm}$  being equal to 0.005 meter. In addition, the radius of curvature ( $R$ ) of the FPS can be written as a function of  $TR$ , which as related in Equation (5).

$$D_{upm} = R - \sqrt{R^2 - D_{Lm}^2} \quad (4)$$

$$R = \left( \frac{TR \times T_1}{2\pi} \right)^2 \times g \quad (5)$$

By combining Equation (4) and (5),  $D_{Lm}$  can be written as a function of  $TR$ :

$$D_{Lm} = \sqrt{0.010 \left( \left( \frac{TR \times T_1}{2\pi} \right)^2 \times g \right) - (D_{upm})^2} \quad (6)$$

where  $g = 9.8 \text{ m/s}^2$  and  $D_{upm} = 0.005 \text{ m}$

**Table 20 The calculated  $D_{Lm}$  [mm] values for each of the TR**

<b>TR</b>	0.5	0.75	1	1.25	1.5	1.75	2	2.25	2.5	2.75	3	3.25	3.5
<b><math>D_{Lm}</math></b>	12	26	39	52	65	78	91	104	117	130	143	156	169